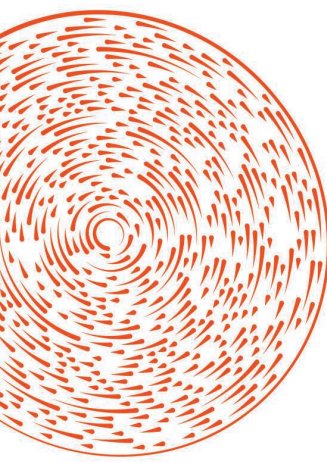




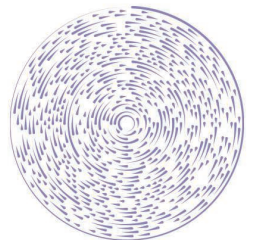
*Qian Gao^{ID},
Mason Ernest Fordham,
Wei Gu^{ID}, Han Cui,
and Yuanxun Ethan Wang^{ID}*

Design RF Magnetic Devices With Linear and Nonlinear Equivalent Circuit Models



Magnetic materials offer a unique combination of properties for RF applications, such as nonreciprocity, high permeability, broad tunability, strong frequency dispersion, and nonlinearity [1]–[3]. In contrast to a dielectric material, where a scalar permittivity constant is often sufficient to represent the property of the material, the permeability of an RF magnetic material is usually a tensor in its linear regime, which

Qian Gao (nancyxixi@g.ucla.edu), Mason Ernest Fordham (mfordham@ucla.edu), and Yuanxun Ethan Wang (ywang@ee.ucla.edu) are with the University of California at Los Angeles, Los Angeles, CA 90095 USA. Wei Gu (gu.william.wei@gmail.com) is with the Beijing Institute of Technology, Beijing 100081, China. Han Cui (helencui@utk.edu) is with the University of Tennessee, Knoxville, TN 37996 USA.



©SHUTTERSTOCK.COM/PIXSSA

Digital Object Identifier 10.1109/MMM.2022.3196414

Date of current version: 4 October 2022

is expressed in the form of an asymmetrical matrix; yet each entry in the matrix varies as a function of frequency and biasing field. At high RF power, the magnetic material can be easily driven into a nonlinear regime, which exhibits increased dissipation, drifting of resonant frequency, generation of harmonics, and so on. At a microscale, electromagnetic waves in magnetic materials are often coupled with spin waves that are supported by exchange coupling in quantum mechanics, which adds more complexity to the understanding and applications of the material.

Because of these unique properties, magnetic materials have been developed for various linear RF devices [4], [5], such as inductors [6], circulators [7]–[10], isolators [11], phase shifters [4], [5], filters [12]–[18], and antennas [19]–[23]. Nonlinear RF magnetic devices, such as frequency-selective limiters (FSLs) and signal-to-noise enhancers, have also received significant attention lately [24]–[32]. Leveraging on the recent advances in the fabrication of thin-film and thick-film magnetic materials, many traditional RF magnetic devices can now be integrated on chip, which opens up ways to supply high-quality-factor passives on chip that are lacking in existing semiconductor-based integrated circuit processes [33]. However, the complex nature of the magnetic material poses significant challenges to the modeling of RF magnetic devices in an accurate, computationally efficient fashion.

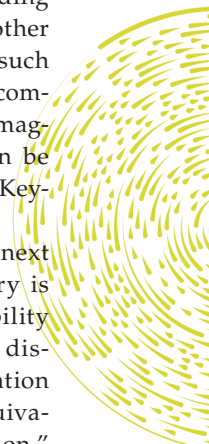
Full-wave modeling tools, such as the high-frequency structure simulator (HFSS) [34], solve Maxwell's equations based on Polder's permeability tensor, but they can neither model the nonlinear property of the magnetic material nor include spin waves where exchange coupling is involved. Micromagnetic simulators, such as the Object Oriented MicroMagnetic Framework or MuMax [35]–[39], solve the nonlinear Landau–Lifshitz–Gilbert (LLG) equation [40] on the micron scale, where magnetostatic approximation can be applied to model the dipole-to-dipole coupling and exchange coupling. Yet, computationally, it is no longer affordable in practical microwave devices when the scale of those interactions reaches millimeters and the full-wave electrodynamic interactions must be considered. Furthermore, despite the great success these modeling efforts have achieved in their respective domains of application, the intuitive understanding of the physics in magnetic materials is often overshadowed by the complexity of the mathematics. From a design perspective, it is also desired to establish unified models between RF electronics and magnetics to facilitate co-designs.

The purpose of this article is to develop a series of equivalent circuit models that can represent the

From a design perspective, it is also desired to establish unified models between RF electronics and magnetics to facilitate co-designs.

dynamic spin precession physics and the propagation of spin waves in magnetic materials for both linear and nonlinear cases. These circuit models will be derived rigorously from micromagnetic theory, i.e., the LLG equation [40]. Yet they describe the impact of material parameters, such as the biasing field, the saturation magnetization, and the material shapes, on the spin precessions in a concise and intuitive manner. The models can also be scaled according to physical dimensions and combined with other equivalent circuit models of practical devices, such as transmission lines and antennas, to create complete equivalent circuit models of these RF magnetic devices. Finally, the device behaviors can be obtained with a circuit simulator, such as the Keysight Advanced Design System (ADS).

This article is organized as follows. In the next section, the fundamental micromagnetic theory is introduced, and the property of the permeability tensor, e.g., Polder's permeability tensor, is discussed by applying the small-signal approximation to the LLG equation. In the section "Linear Equivalent Circuit Model for Dynamic Spin Precession," a linear equivalent circuit model representing dynamic spin precession is derived, which replicates the result of the Polder permeability tensor. The model is then integrated into a microstripline model or an electrically small antenna model to predict the input impedance of the microstripline, which is loaded with an yttrium iron garnet (YIG) thin film [41], and the input impedance as well as the radiation efficiency of an electrically small loop antenna loaded with a YIG thin film. In the section "Nonlinear Equivalent Circuit Model for Dynamic Spin Precession," a nonlinear equivalent circuit model is derived from the original, nonlinear LLG equation and applied to predict the nonlinear spin precession behaviors for both a YIG sphere and a YIG thin film. In the section "Equivalent Circuit Models for Magnetostatic Waves and Spin Waves," equivalent circuit models representing the propagation of magnetostatic waves and spin waves [42], [43] are proposed. In the section "Nonlinear Equivalent Circuit Model for FSLs," the derived spin-wave equivalent circuits are combined with the nonlinear spin precession models to predict the nonlinear behaviors of FSLs in a way similar to the methods of [44]–[47].



Micromagnetic Theory

From quantum mechanics theory, the origin of magnetism is understood as the orderly motions of electron spins. The classical treatment of electron spin precession in a magnetic material is through the equation of motion,

$$\frac{d\mathbf{M}}{dt} = -\mu_0\gamma\mathbf{M} \times \mathbf{H}, \quad (1)$$

where \mathbf{M} is the magnetic dipole moment, \mathbf{H} is the total magnetic field, μ_0 is the free space permeability, and γ is the gyromagnetic ratio of the electron. The equation of motion can be generalized to describe the dynamic behaviors of magnetization in a magnetic material, where \mathbf{M} is now defined as the magnetization vector at a given observation location and \mathbf{H} as the total effective magnetic field at the location, which consists of the applied field, demagnetization field, anisotropic field, and exchange field according to their different physics origins, i.e., [1], [2], [40]

$$\mathbf{H} = \mathbf{H}_{\text{appl}} + \mathbf{H}_{\text{demag}} + \mathbf{H}_{\text{anis}} + \mathbf{H}_{\text{ex}}. \quad (2)$$

The first two types of fields are of Maxwellian origin. The applied field is the incident field from an external source, such as a current, and the demagnetization field represents the interactions among the magnetic dipoles inside the material (dipole-to-dipole interactions). The demagnetization field is often approximated as magnetostatic interactions in a traditional micromagnetic length scale ($<10 \mu\text{m}$), but it could be more precisely modeled by electrodynamics over a longer scale. The last two types of fields are of atomic origin. The anisotropic field results from the spin-orbit coupling that forces the spins oriented toward certain crystallographic axes of the material, and the exchange field represents the exchange coupling, which originates from Heisenberg interactions in quantum mechanics. It should be noted that the thermal fluctuation field is ignored in (2) as it is often much weaker than the four fields listed in (2). However, as will be elaborated later, the existence of the thermal field is necessary for nonlinear RF magnetic devices, such as FSLs, to work because a noise input is required for the excitation of the spin-wave oscillations in such devices.

When loss of the material due to the damping of the spin precession is considered, the equation of motion in (1) can be modified by including a damping term, resulting in the LLG equation

$$\frac{\partial\mathbf{M}}{\partial t} = -\mu_0\gamma\mathbf{M} \times \mathbf{H} + \frac{\alpha}{M_s}\mathbf{M} \times \frac{\partial\mathbf{M}}{\partial t}, \quad (3)$$

where α is the Gilbert damping constant and M_s is the saturation magnetization of the material. Expanding the LLG equation to its scalar form yields

$$\frac{\partial M_x}{\partial t} = -\mu_0\gamma(M_y H_z - M_z H_y) + \frac{\alpha}{M_s}\left(M_y \frac{\partial M_z}{\partial t} - M_z \frac{\partial M_y}{\partial t}\right), \quad (4a)$$

$$\frac{\partial M_y}{\partial t} = -\mu_0\gamma(M_z H_x - M_x H_z) + \frac{\alpha}{M_s}\left(M_z \frac{\partial M_x}{\partial t} - M_x \frac{\partial M_z}{\partial t}\right), \quad (4b)$$

$$\frac{\partial M_z}{\partial t} = -\mu_0\gamma(M_x H_y - M_y H_x) + \frac{\alpha}{M_s}\left(M_x \frac{\partial M_y}{\partial t} - M_y \frac{\partial M_x}{\partial t}\right) \quad (4c)$$

When the LLG equation is applied to a spatial cell where uniform magnetization is assumed, the conservation of magnetization holds, i.e.,

$$M_s = \sqrt{M_x^2 + M_y^2 + M_z^2}. \quad (5)$$

For most RF and microwave applications, a magnetic material, such as ferrite, is operated under a strong dc biasing field that saturates the material in one direction. This is done to prevent the formation of domains in magnetic material and energy loss associated with the rotation of domains under the influence of the RF field. The dc biasing field can be applied externally with a coil or a permanent magnet. It can also be applied by the internal anisotropic field of the material, which is called *self-biasing*. The total effective magnetic field can thus be separated into a dc component superimposed with an RF component as

$$\mathbf{H} = H_0\hat{z} + \mathbf{h} \quad (6)$$

where H_0 is the dc biasing field and \mathbf{h} is the RF field vector.

Note that the LLG equation is a nonlinear equation that involves the product of the magnetization vector and the magnetic field. With magnetocrystalline anisotropy and exchange coupling ignored, a small-signal approximation can be introduced by assuming $|\mathbf{h}| \ll H_0$ and $M_z = M_s$, which leads to the linearized LLG equation in the following form:

$$\frac{\partial M_x}{\partial t} = -\mu_0\gamma(M_y H_0 - M_s h_y) - \alpha \frac{\partial M_y}{\partial t}, \quad (7a)$$

$$\frac{\partial M_y}{\partial t} = \mu_0\gamma(M_x H_0 - M_s h_x) + \alpha \frac{\partial M_x}{\partial t}, \quad (7b)$$

$$\frac{\partial M_z}{\partial t} = 0. \quad (7c)$$

Transforming (7a) and (7b) into the frequency domain yields

$$j\omega\tilde{M}_x = -(\omega_0 + j\omega\alpha)\tilde{M}_y + \omega_m\tilde{h}_y, \quad (8a)$$

$$j\omega\tilde{M}_y = (\omega_0 + j\omega\alpha)\tilde{M}_x - \omega_m\tilde{h}_x, \quad (8b)$$

where ω is the operating angular frequency, and $\omega_0 = \mu_0 \gamma H_0$ and $\omega_m = \mu_0 \gamma M_s$ are the angular frequency equivalents of the biasing field and the saturation magnetization.

The solution of the previous linearized LLG equation for unbound ferrite can be easily obtained by solving (8a) and (8b), which yields a frequency-dispersive, anisotropic susceptibility tensor,

$$\begin{bmatrix} \tilde{M}_x \\ \tilde{M}_y \end{bmatrix} = \begin{bmatrix} \chi_{xx} & \chi_{xy} \\ \chi_{yx} & \chi_{yy} \end{bmatrix} \begin{bmatrix} \tilde{H}_x \\ \tilde{H}_y \end{bmatrix}, \quad (9)$$

where

$$\begin{aligned} \chi_{xx} = \chi_{yy} &= \frac{(\omega_0 + j\alpha\omega)\omega_m}{(\omega_0 + j\alpha\omega)^2 - \omega^2} \\ &= \frac{\omega_m}{\omega_0} \frac{\omega_0^2 + j\alpha\omega\omega_0}{\omega_0^2 - (1 + \alpha^2)\omega^2 + 2j\alpha\omega\omega_0}, \end{aligned} \quad (10a)$$

$$\begin{aligned} \chi_{xy} = -\chi_{yx} &= \frac{j\omega\omega_m}{(\omega_0 + j\alpha\omega)^2 - \omega^2} \\ &= \frac{\omega_m}{\omega_0} \frac{j\omega\omega_0}{\omega_0^2 - (1 + \alpha^2)\omega^2 + 2j\alpha\omega\omega_0} \end{aligned} \quad (10b)$$

constitute what is called Polder's susceptibility tensor, which is often used by RF and microwave engineers [1], [2], [48]. The susceptibility starts from an initial value of ω_m/ω_0 at around the dc and reaches a resonance peak around the frequency ω_0 , i.e., its ferromagnetic resonance frequency (FMR).

For a magnetic material with a finite geometry, the demagnetization field must be considered. Under the magnetostatic scale limit, the demagnetization field can be approximated by

$$H_{\text{demag}} = -N \cdot M, \quad (11)$$

where N is the demagnetization factor [1], [2]. For ferrite plates or thin films whose out-of-plane direction is along the biasing axis (the z -axis), a demagnetization field must be applied in the opposite direction of the biasing, which reduces the effective biasing field in the material to $H_0 - M_s$. Polder's susceptibility tensor can be obtained in the same form by simply substituting the relation $\omega_0 = \mu_0 \gamma (H_0 - M_s)$ in (10). For ferrite plates or thin films with an in-plane biasing in the z -axis and an out-of-plane direction in the y -axis, the demagnetization field becomes part of the RF field. The linearized LLG equation (8) thus becomes

$$j\omega\tilde{M}_x = -(\omega_0 + j\alpha\omega)\tilde{M}_y + \omega_m(\tilde{h}_{y,\text{appl}} - \tilde{M}_y), \quad (12a)$$

$$j\omega\tilde{M}_y = (\omega_0 + j\alpha\omega)\tilde{M}_x - \omega_m\tilde{h}_{x,\text{appl}}. \quad (12b)$$

This implies that the in-plane biased thin film ferrite may be more appropriate for RF and microwave applications because of the lower required biasing field to reach a high FMR and thus a higher initial permeability.

When an external RF magnetic field is applied only to the x -axis, the resulting magnetization susceptibility is given by

$$\chi_{xx} = \frac{\tilde{M}_x}{\tilde{h}_{x,\text{appl}}} = \frac{\omega_m}{\omega_0} \frac{\omega_r^2 + j\alpha\omega\omega_0}{\omega_r^2 - (1 + \alpha^2)\omega^2 + j\alpha\omega(2\omega_0 + \omega_m)}, \quad (13)$$

where ω_r is the thin-film FMR, which is given by

$$\omega_r = \sqrt{\omega_0(\omega_0 + \omega_m)}. \quad (14)$$

Comparing (13) to (10), it is evident that the FMR of the thin-film ferrite is much higher than that of the unbound ferrite, when $\omega_m \gg \omega_0$. The initial susceptibility and the shape of the susceptibility dispersion remain similar for both cases. This implies that the in-plane biased thin-film ferrite may be more appropriate for RF and microwave applications because of the lower required biasing field to reach a high FMR and thus a higher initial permeability.

Linear Equivalent Circuit Model for Dynamic Spin Precession

The rationale of representing the behavior of a magnetic material with equivalent circuit models is established based upon Maxwell's equations. Faraday's law indicates that the electromotive force, a form of voltage, is the time-rate change of the magnetic flux. Similarly, the current can be related to the magnetic field through Ampere's law, although a conductive current does not physically exist in most ferrite materials. To illustrate this concept, one may consider the cubic cell within an unbound volume of ferrite shown in Figure 1. The cell has dimensions of Δx , Δy , and Δz along the x -, y -, and z -axes. The dc biasing field is applied to the z -axis. Applying Faraday's law, the electromotive force (EMF) around the perimeter of the surface $\Delta y \times \Delta z$ denoted by V^x is related to the x -component of the dynamic magnetization vector by

$$V^x = \mu_0 \frac{\partial M_x}{\partial t} \Delta y \Delta z. \quad (15)$$

The rationale of representing the behavior of a magnetic material with equivalent circuit models is established based upon Maxwell's equations.

On the other hand, the current flowing crossing the x -axis, toward either the y - or the z -axis, must have a contribution from the x -component of the Maxwellian magnetic field according to Ampere's law. This contribution can be denoted by

$$I^x = H_x \Delta x. \quad (16)$$

Note that in (15) the voltage is EMF, and in (16) the current is a fraction of a real current. Superscripts are thus used to differentiate them from physically measurable voltage or current along the x -direction. Equations (15) and (16) are called *field-to-circuit*

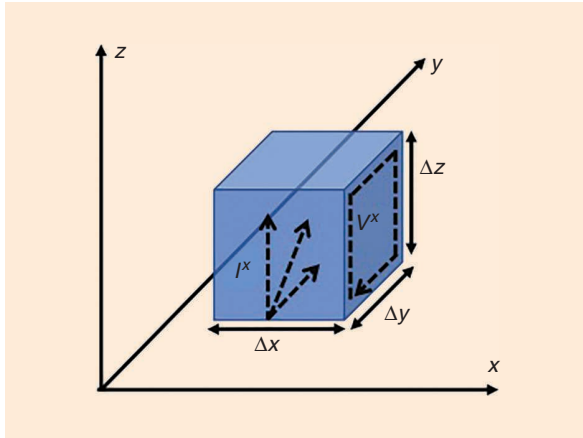


Figure 1. A cuboid cell in ferrite where the correspondence of the field variables (H , M) to the circuit variables (I , V) is established.

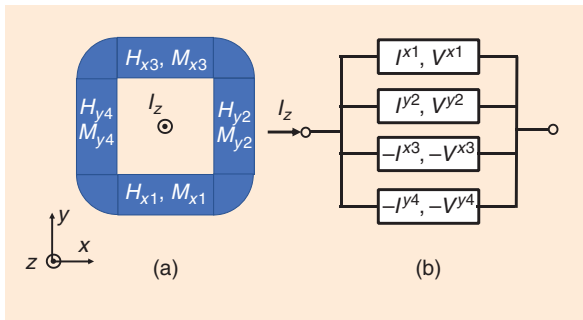


Figure 2. (a) An example with a current filament through a ferrite ring. (b) Its equivalent circuit consisting of four ferrite cuboid cell models in parallel sharing the same input current of the current filament.

transformations. Equivalent circuits for magnetic materials can thus be defined between the voltage and current expressed in (15) and (16); yet such circuits for magnetic materials cannot be connected to conventional electrical circuits through simple connections of voltage and current nodes. To interface with the conventionally defined voltage and current nodes in nonmagnetic circuits, a number of ferrite cuboid cell models may be needed, while the current continuity and voltage continuity are enforced by Ampere's law and the flux continuity condition, respectively. An example is a z -directed current filament with a total current of I_z penetrating through a ferrite ring, as shown in Figure 2(a). Ignoring the four corners, the ferrite is represented by the four cuboids around the current filament. Ampere's law thus gives

$$\begin{aligned} I_z &= H_{x1} \Delta x + H_{y2} \Delta y - H_{x3} \Delta x - H_{y4} \Delta y \\ &= I^{x1} + I^{y2} - I^{x3} - I^{y4}. \end{aligned} \quad (17)$$

On the other hand, the flux continuity condition is enforced:

$$M_{x1} \Delta y \Delta z = M_{y2} \Delta x \Delta z = -M_{x3} \Delta y \Delta z = -M_{y4} \Delta x \Delta z, \quad (18)$$

which is equivalent to the voltage continuity:

$$V^{x1} = V^{y2} = -V^{x3} = -V^{y4}. \quad (19)$$

The equivalent circuit of the structure is thus yielded, as shown in Figure 2(b), which consists of four ferrite cuboid cell models in parallel that share the total amount of current I_z .

Applying the field-to-circuit transformations for all magnetization and magnetic field components, the linearized LLG equations (7a) and (7b) can now be rewritten as circuit equations:

$$\frac{1}{\mu_0} \frac{V^x}{\Delta y \Delta z} = -\frac{1}{\mu_0} \frac{\omega_0}{\Delta x \Delta z} \int V^y dt + \frac{\omega_m I^y}{\Delta y} - \alpha \frac{1}{\mu_0} \frac{V^y}{\Delta x \Delta z} \quad (20a)$$

$$\frac{1}{\mu_0} \frac{V^y}{\Delta x \Delta z} = \frac{1}{\mu_0} \frac{\omega_0}{\Delta y \Delta z} \int V^x dt - \frac{\omega_m I^x}{\Delta x} + \alpha \frac{1}{\mu_0} \frac{V^x}{\Delta y \Delta z} \quad (20b)$$

Rewriting (20a) and (20b) by multiplying both sides of the equations by $\Delta y / \omega_m$ and $\Delta x / \omega_m$, respectively, yields

$$\frac{1}{\mu_0 \omega_m \Delta z} V^x = -\frac{1}{\mu_0} \frac{\omega_0}{\omega_m} \frac{\Delta y}{\Delta x \Delta z} \int V^y dt + I^y - \frac{\alpha}{\mu_0 \omega_m} \frac{\Delta y}{\Delta x \Delta z} V^y, \quad (21a)$$

$$-\frac{1}{\mu_0 \omega_m \Delta z} V^y = -\frac{1}{\mu_0} \frac{\omega_0}{\omega_m} \frac{\Delta x}{\Delta y \Delta z} \int V^x dt + I^x - \frac{\alpha}{\mu_0 \omega_m} \frac{\Delta x}{\Delta y \Delta z} V^x, \quad (21b)$$

or

$$I^y = \frac{\int V^y dt}{L_y} + \frac{V^y}{R_y} + \frac{V^x}{Z_g} = I_{L_y} + I_{R_y} + I_{C_y}, \quad (22a)$$

$$I^x = \frac{\int V^x dt}{L_x} + \frac{V^x}{R_x} - \frac{V^y}{Z_g} = I_{L_x} + I_{R_x} - I_{G_x}, \quad (22b)$$

with $Z_g, L_x, L_y, R_x,$ and R_y defined as follows:

$$\begin{cases} Z_g = \mu_0 \omega_m \Delta z = \mu_0^2 \gamma M_s \Delta z \\ L_x = \mu_0 \frac{\omega_m}{\omega_0} \frac{\Delta y \Delta z}{\Delta x} = \mu_0 \frac{M_s}{H_0} \frac{\Delta y \Delta z}{\Delta x} \\ L_y = \mu_0 \frac{\omega_m}{\omega_0} \frac{\Delta x \Delta z}{\Delta y} = \mu_0 \frac{M_s}{H_0} \frac{\Delta x \Delta z}{\Delta y} \\ R_x = \mu_0 \frac{\omega_m}{\alpha} \frac{\Delta y \Delta z}{\Delta x} = \frac{\mu_0^2 \gamma M_s}{\alpha} \frac{\Delta y \Delta z}{\Delta x} \\ R_y = \mu_0 \frac{\omega_m}{\alpha} \frac{\Delta x \Delta z}{\Delta y} = \frac{\mu_0^2 \gamma M_s}{\alpha} \frac{\Delta x \Delta z}{\Delta y} \end{cases}. \quad (23)$$

Considering the left-hand side of (22) as an incident current and the three terms on the right-hand side as currents flowing into an inductor I_{L_x} or I_{L_y} and a resistor I_{R_x} or I_{R_y} and a gyrator I_{G_x} or I_{G_y} , respectively, it is evident that (22) represents a two-port circuit with each of the ports loaded by a resistor and an inductor while the two ports are coupled through a gyrator, as shown in Figure 3, where Z_g is the impedance of the gyrator, and $L_x, L_y, R_x,$ and R_y represent the values of the loaded inductors and resistors for both the x -port and y -port. The use of the gyrator in the equivalent circuit is to model the nonreciprocity of the magnetic material, and the sign of the gyrator determines the right-hand rotation characteristics of the spin precessions. Note that a similar gyrator/inductor model was proposed in [12] to represent the coupling of two coils through a YIG sphere. That model, however, did not define the circuit parameters based on the material parameters, nor did it include the resistors to represent the Gilbert damping in the magnetic material.

For thin-film ferrites, the out-of-plane (y -axis) demagnetization must be considered. Equation (11) gives $h_y = -M_y$, which serves as an inductive termination

boundary condition for the y -port under the field-to-circuit transformations (15) and (16); i.e.,

$$I^y = h_y \Delta y = -M_y \Delta y = -\frac{1}{\mu_0} \frac{\Delta y}{\Delta x \Delta z} \int V^y dt = -\frac{\int V^y dt}{L_d}, \quad (24)$$

where the demagnetization inductance L_d is given by

$$L_d = \mu_0 \frac{\Delta x \Delta z}{\Delta y}. \quad (25)$$

The circuit model can thus be modified by simply adding this demagnetization inductor as a load at the y -port. If only the x -polarized RF magnetics behavior is considered, the input impedance of the x -port can be obtained with the inductive loads at the y -port transformed to a capacitive load through the gyrator, forming a parallel RLC resonator, as illustrated in Figure 4.

The transformed capacitance C_x is given by

$$C_x = \frac{L_y \parallel L_d}{Z_g^2} = \frac{1}{\mu_0 (\omega_m + \omega_0) \omega_m} \frac{\Delta x}{\Delta y \Delta z}. \quad (26)$$

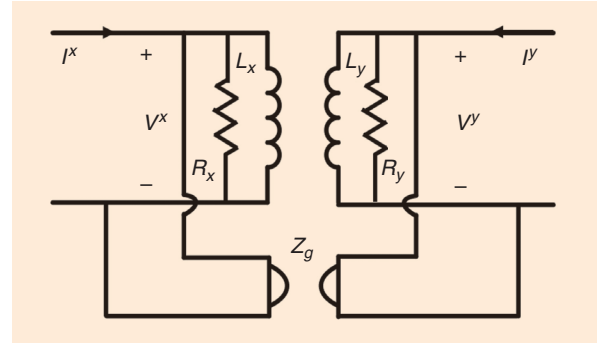


Figure 3. An equivalent circuit derived for a biased magnetic material cell representing its linear, dynamic, and nonreciprocal magnetization behavior.

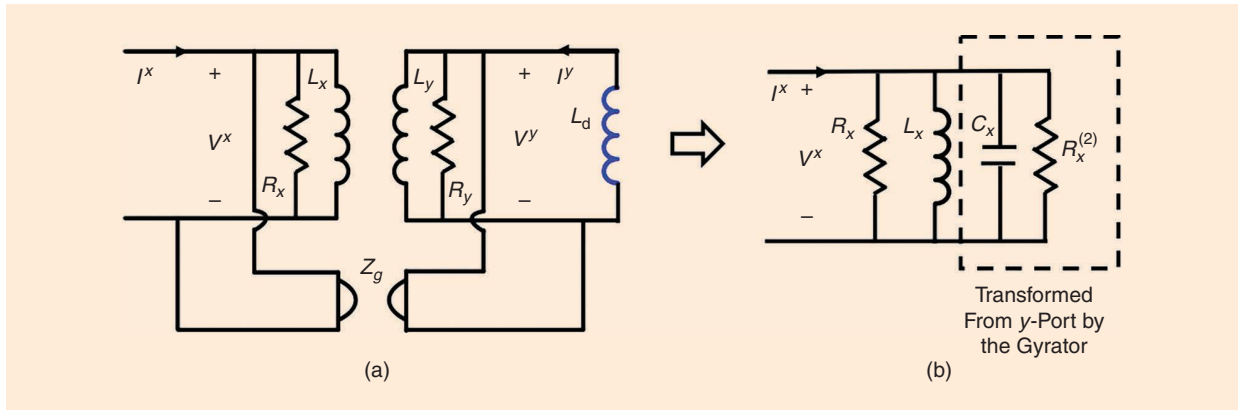


Figure 4. (a) Inclusion of the out-of-plane demagnetization effect (y -axis as shown) in the gyrator coupled inductor model and (b) its equivalence to a parallel RLC model.

For longitudinally biased microstrip or striplines loaded with ferrite films or substrates, a complete equivalent circuit can be obtained by modifying that of the nonmagnetic microstrip or stripline.

It can be shown that the capacitance C_x resonates with the inductance L_x at the thin-film FMR frequency given by (14). The damping resistance at the y -port is also transformed to be at the x -port with the value at the proximity of the FMR,

$$R_x^{(2)} = \frac{Q^2 Z_g^2}{R_y} = \mu_0 \frac{\omega_m (\omega_m + \omega_0)^2}{\alpha \omega^2} \frac{\Delta y \Delta z}{\Delta x} \approx \mu_0 \frac{\omega_m (\omega_m + \omega_0)}{\alpha \omega_0} \frac{\Delta y \Delta z}{\Delta x}, \quad (27)$$

where Q is the quality factor of the y -port inductance; i.e., $Q = R_y / \omega (L_y \parallel L_d) = (\omega_m + \omega_0) / (\alpha \omega)$. The total damping resistance of the x -port RLC resonator now yields

$$R_x^t = R_x \parallel R_x^{(2)} = \mu_0 \frac{\omega_m (\omega_m + \omega_0)}{\alpha (2\omega_0 + \omega_m)} \frac{\Delta y \Delta z}{\Delta x}. \quad (28)$$

The thin-film ferrite model derived through the field-to-circuit transformation agrees with that in [14], where the circuit model is derived based on fitting of the dispersive characteristic impedance of a ferrite-loaded parallel-plate waveguide. The equivalent circuit model of the magnetic material offers a unique capability of designing RF electronic devices loaded with magnetic materials as the model can be directly integrated into the equivalent circuits of electronics. Next we will demonstrate such examples, e.g., using the derived equivalent circuit model for the design of microwave resonators and electrically small antennas.

Thin-Film YIG-Loaded Microstrip Resonator

The FMR behavior of ferrite has long been used to develop tunable filters [4], [5], [12]–[18] as the resonance frequency of ferrite can be tuned over a broadband by changing the magnetic biasing field. For longitudinally biased microstrip or striplines loaded with ferrite films or substrates, a complete equivalent circuit can be obtained by modifying that of the nonmagnetic microstrip or stripline. As shown in Figure 5, the nonmagnetic transmission lines can be modeled by the well-known series inductor and shunt capacitor ladder circuits, with each LC ladder representing a segment of the transmission line whose length is much shorter than the wavelength of the electromagnetic wave. Assuming that the width of the microstrip is much greater than its thickness so that a parallel-plate model applies, the values of the LC components are given by

$$\begin{cases} L_0 = \mu_0 \frac{\Delta y \Delta z}{\Delta x} \\ C_0 = \epsilon \frac{\Delta x \Delta z}{\Delta y} \end{cases}. \quad (29)$$

Assuming the magnetic field within each segment of transmission line is uniform, and the current flowing on the stripline is longitudinal I_z , it is not difficult to prove that $I^x = I_z$. Δx , Δy , and Δz are, respectively, the width, thickness, and length of this segment. The loading of the ferrite substrate can then be represented by inserting a parallel RLC tank in Figure 4(b) in series with the original ladder inductor, as shown in Figure 5; the values can be derived as

$$\begin{cases} L_m = \mu_0 \frac{\omega_m}{\omega_0} \frac{\Delta y \Delta z}{\Delta x} = \mu_0 \frac{M_s}{H_0} \frac{\Delta y \Delta z}{\Delta x} \\ C_m = \frac{1}{\mu_0 (\omega_m + \omega_0) \omega_m} \frac{\Delta x}{\Delta y \Delta z} = \frac{1}{\mu_0^3 \gamma^2 (M_s + H_0) M_s} \frac{\Delta x}{\Delta y \Delta z} \\ R_m = \mu_0 \frac{\omega_m (\omega_m + \omega_0)}{\alpha (2\omega_0 + \omega_m)} \frac{\Delta y \Delta z}{\Delta x} = \mu_0^2 \gamma \frac{M_s (M_s + H_0)}{\alpha (2H_0 + M_s)} \frac{\Delta y \Delta z}{\Delta x} \end{cases} \quad (30)$$

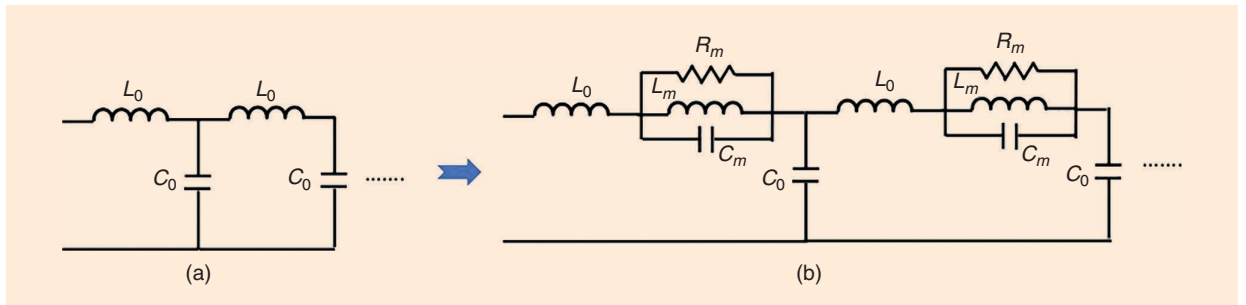


Figure 5. (a) The LC ladder circuit equivalence of a nonmagnetic transmission line. (b) The series L , shunt C unit cell is modified by adding a parallel RLC tank for an equivalent circuit of the magnetic transmission line with a biased ferrite substrate.

The resonance frequency is thus given by

$$\omega_r = \frac{1}{\sqrt{L_m C_m}} = \mu_0 \gamma \sqrt{H_0 (H_0 + M_s)} = \sqrt{\omega_0 (\omega_0 + \omega_m)}, \quad (31)$$

which agrees with (14).

A short-circuited magnetic transmission line bypasses the capacitor in Figure 5(b), and the structure can thus be equivalent to the parallel RLC tank that represents the FMR, in series with the inductor L_0 that represents the inductance of air. When the Q of the RLC resonator is high or L_m is much greater than L_0 , the impact of the air inductance can be ignored, and an RLC resonator with its resonant frequency tunable by the magnetic biasing field is yielded that can be used as a building block of a tunable filter. Figure 6 illustrates

such a stripline structure with a length of 0.5 mm and width of 100 μm , sandwiched by two 3- μm -thick YIG films. The structure is simulated in HFSS, and its input impedance is compared to that of the RLC plus inductor model, as shown in Figure 6(b). The impedance result shows very good agreement in Figure 7, where the HFSS prediction is plotted against the result of the circuit model. Both the resonant frequency and its line-width are correctly predicted by the circuit model.

Thin-Film YIG-Loaded Electrically Small Loop Antenna

Electrically small loop antennas are among the simplest antennas. As the radiation resistance of a single-turn loop is usually small, multiple turns are often

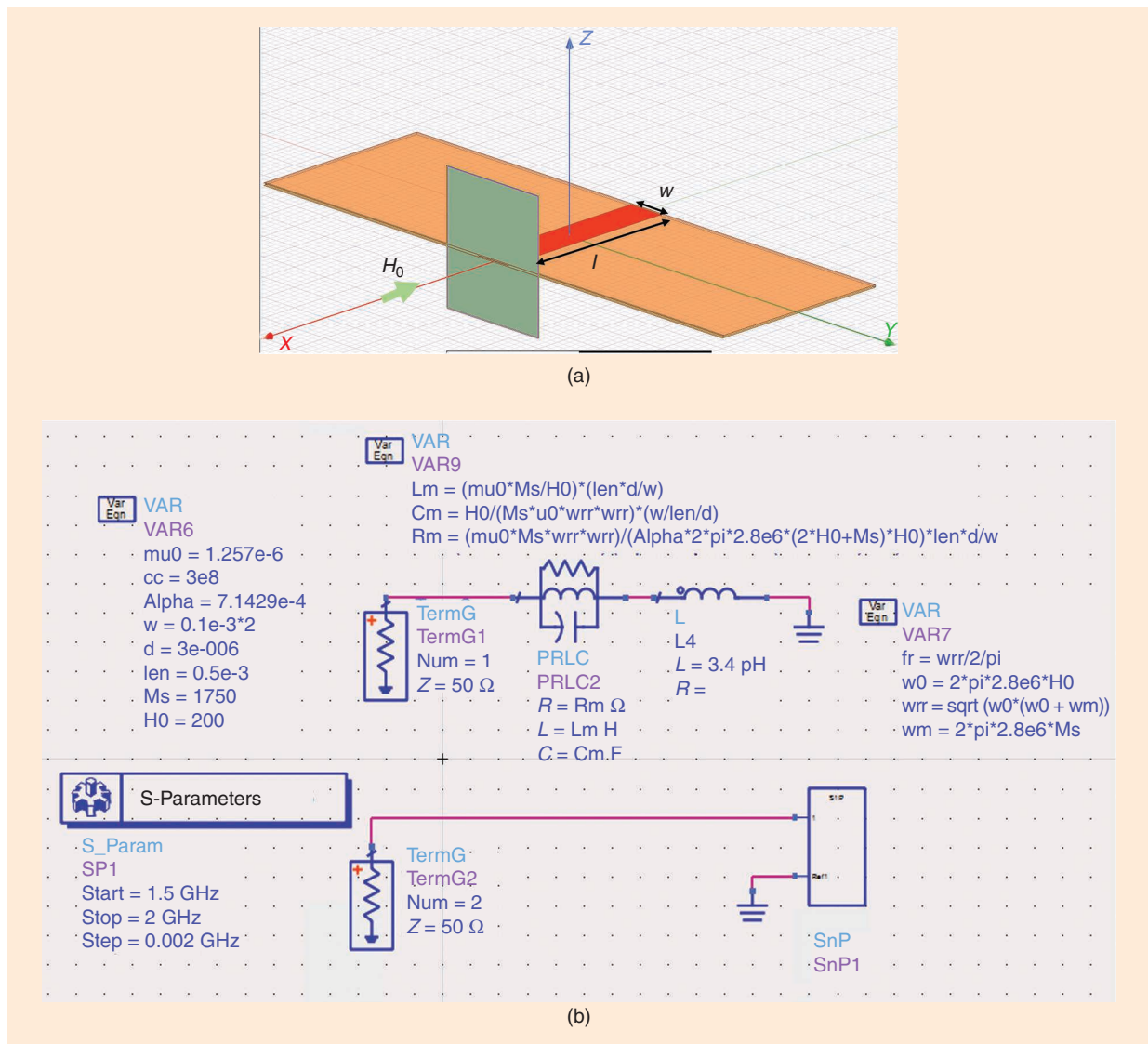


Figure 6. (a) A short-circuited stripline with a width of 100 μm and length of 0.5 mm sandwiched by two 3- μm -thick YIG films that is longitudinally biased, simulated in HFSS. (b) The ADS setup for comparison between the S-parameter derived from HFSS and the analytically derived equivalent circuit model.

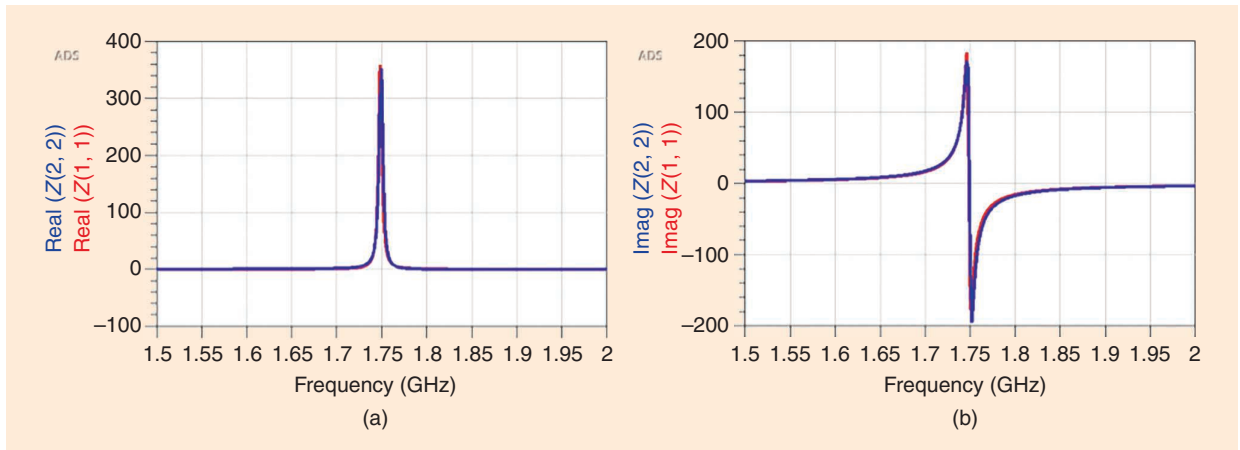


Figure 7. An input impedance comparison as a function of frequency between the HFSS simulations (red line) and the prediction of the circuit model (blue line). (a) Input resistance. (b) Input reactance.

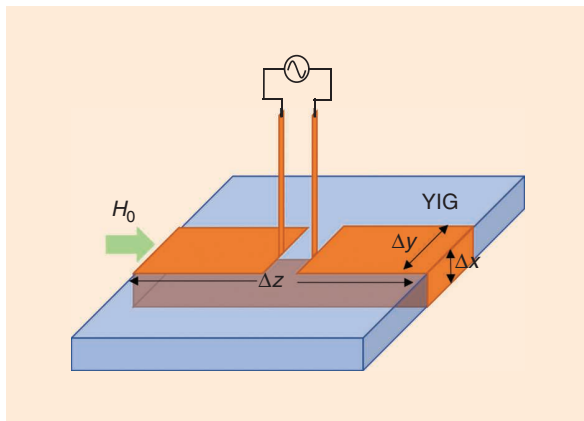


Figure 8. A single-turn loop antenna loaded with thin-film YIG biased longitudinally as shown.

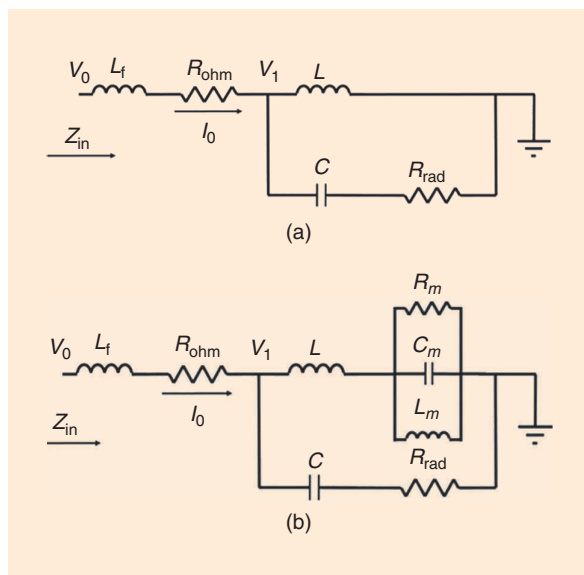


Figure 9. Equivalent circuit models for electrically small loops (a) without ferrite and (b) with ferrite (FMR). (Source: [23].)

introduced to obtain an impedance that matches to standard electronics. The increase of the radiation resistance through winding, however, often comes at the price of increased ohmic resistance and parasitic capacitance. It is proposed in [23] to use the high-Q FMR of a thin-film YIG to increase the input impedance of a single-turn loop. The proposed antenna is a single-turn stripe wrapped around a thin-film YIG substrate, as shown in Figure 8. The ferrite substrate is a 3.08- μm -thick YIG film epitaxially deposited on a 500- μm -thick gadolinium gallium garnet substrate. Its length and width are 6 mm and 5 mm, respectively. The conducting loop is designed to be at the same width of 6 mm. A dc magnetic bias field H_0 of 36 Oe (2,865 A/m) parallel to the current flow is assigned. The FMR-enhanced electrically small loop is designed to operate at around 0.7 GHz. What must be emphasized here is that this antenna is extremely small in its electrical size; its largest physical dimension is approximately 1/60 of its operating wavelength.

To better understand the role FMR played, equivalent circuit models are derived for electrically small loop antennas first without and then with the thin-film ferrite. The model of the loop without ferrite is established based on the first order (TE_1) spherical wave model developed by Chu [49] so that the stored energy (parasitics) and the radiation of the lossless electrically small loop can be precisely captured. As shown in Figure 9(a), the inductance L represents the inductive energy stored in the loop antenna. The radiation resistance R_{rad} is placed at a different branch in parallel to this inductor. An ohmic resistance R_{ohm} is in series with the lossless circuit model to include the power dissipated on the conducting loop structure.

It should be noted that, in the model shown in Figure 8(a), an inductance L_f is also added in front of R_{ohm}

to model the parasitic effect of the feeding lines. For the loop antenna with the loading of the thin-film ferrite, similar to what is done in the section “Thin-Film YIG-Loaded Microstrip Resonator,” the ferrite can be represented by the insertion of a parallel RLC tank, in series with the loop inductor L , as shown in Figure 9(b), as the magnetic flux of the biased thin-film YIG generates an EMF in addition to that of the original air loop inductance. The value of the RLC elements can be approximately obtained with (30) by treating the entire antenna as a cuboid ferrite cell with dimensions $\Delta x = 3.08 \mu\text{m}$, $\Delta y = 6 \text{ mm}$, and $\Delta z = 5 \text{ mm}$, as indicated in Figure 8. After some optimization, the equivalent circuit model presented in Figure 9(a) fits well with the full-wave simulation results of the electrically small loop without

What must be emphasized here is that this antenna is extremely small in its electrical size; its largest physical dimension is approximately 1/60 of its operating wavelength.

ferrite. By just inserting the parallel RLC resonator into the circuit without altering the other parameters, the equivalent circuit model then predicts the behavior of the ferrite-loaded electrically small loop very well, which implies the role of the ferrite or FMR is well represented by the parallel RLC model.

A comparison of the simulated input impedances between the circuit model prediction and HFSS full-wave simulations is shown in Figure 10. The comparison can also be extended to the prediction of radiation efficiency in Figure 11. Good matches between the circuit model and the full-wave simulation results for cases both with and without ferrite have been observed. The simulation results show that the input impedance rises from 1 W to 118 W after the loading of ferrite. The radiation efficiency of the antenna has also experienced a factor of 10 increase from 0.0013% to 0.013% at an FMR frequency of 0.7 GHz.

Nonlinear Equivalent Circuit Model for Dynamic Spin Precession

While the linear gyrator coupled inductor model or the parallel RLC model represents the FMR behavior of ferrite very well, the small-signal approximation of

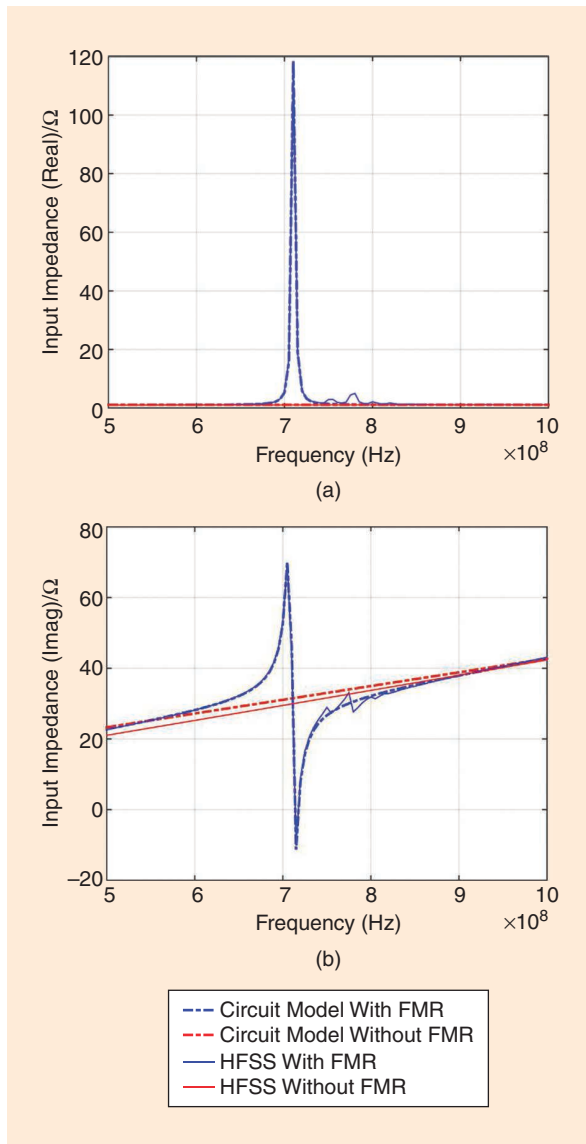


Figure 10. (a) The input resistance and (b) input reactance with and without FMR enhancement: HFSS versus circuit model. (Source: [23].)

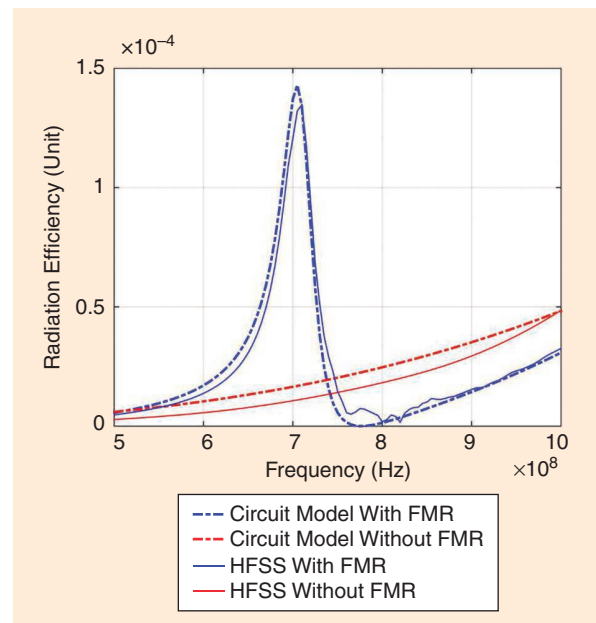


Figure 11. Radiation efficiency with and without FMR enhancement: HFSS versus Circuit Model. (Source: [23].)

$H_z = H_0$ and $M_z = M_s$ no longer holds under the large-signal excitation. It necessitates the use of the LLG equation in (4) in its original, nonlinear form. Taking a time derivative of the conservation of the magnetization condition in (5) yields

$$M_x \frac{\partial M_x}{\partial t} + M_y \frac{\partial M_y}{\partial t} + M_z \frac{\partial M_z}{\partial t} = 0, \quad (32)$$

which can be rewritten as

$$\frac{\partial M_z}{\partial t} = - \left(\frac{M_x}{M_z} \frac{\partial M_x}{\partial t} + \frac{M_y}{M_z} \frac{\partial M_y}{\partial t} \right). \quad (33)$$

Substituting (33) into the $M_x \partial M_z / \partial t$ and $M_y \partial M_z / \partial t$ terms in (4a) and (4b) yields

$$\begin{aligned} \frac{\partial M_x}{\partial t} = & -\mu_0 \gamma (M_y H_z - M_z H_y) \\ & - \frac{\alpha}{M_s} \left[\frac{M_x M_y}{M_z} \frac{\partial M_x}{\partial t} + \left(\frac{M_y^2}{M_z^2} + 1 \right) M_z \frac{\partial M_y}{\partial t} \right], \end{aligned} \quad (34a)$$

$$\begin{aligned} \frac{\partial M_y}{\partial t} = & -\mu_0 \gamma (M_z H_x - M_x H_z) \\ & + \frac{\alpha}{M_s} \left[\frac{M_x M_y}{M_z} \frac{\partial M_y}{\partial t} + \left(\frac{M_x^2}{M_z^2} + 1 \right) M_z \frac{\partial M_x}{\partial t} \right], \end{aligned} \quad (34b)$$

where H is the Maxwellian magnetic field when exchange coupling and dynamic anisotropic field are ignored. For z-biased ferrite, it is reasonable to assume that $|M_x|, |M_y| \ll |M_z|$, which leads to the following approximation:

$$\frac{\partial M_x}{\partial t} = -\mu_0 \gamma (M_y H_z - M_z H_y) - \frac{\alpha}{M_s} M_z \frac{\partial M_y}{\partial t}, \quad (35a)$$

$$\frac{\partial M_y}{\partial t} = -\mu_0 \gamma (M_z H_x - M_x H_z) + \frac{\alpha}{M_s} M_z \frac{\partial M_x}{\partial t}. \quad (35b)$$

Rewriting these two equations yields

$$H_y = \frac{H_z}{M_z} M_y + \frac{\alpha}{\mu_0 \gamma M_s} \frac{\partial M_y}{\partial t} + \frac{1}{\mu_0 \gamma M_z} \frac{\partial M_x}{\partial t}, \quad (36a)$$

$$H_x = \frac{H_z}{M_z} M_x + \frac{\alpha}{\mu_0 \gamma M_s} \frac{\partial M_x}{\partial t} - \frac{1}{\mu_0 \gamma M_z} \frac{\partial M_y}{\partial t}. \quad (36b)$$

A nonlinear circuit equivalence, therefore, applies in a similar manner to how it was done in the linear case, yielding

$$I^y = \frac{\int V^y dt}{L_y} + \frac{V^y}{R_y} + \frac{V^x}{Z_g} = I_{Ly} + I_{Ry} + I_{Gy}, \quad (37a)$$

$$I^x = \frac{\int V^x dt}{L_x} + \frac{V^x}{R_x} - \frac{V^y}{Z_g} = I_{Lx} + I_{Rx} - I_{Gx}. \quad (37b)$$

Note that each term on the right-hand side of (37) represents a current flowing through an inductor, a resistor, and a gyrator, with Z_g , L_x , L_y , R_x , and R_y defined as follows:

$$\begin{cases} Z_g = \mu_0^2 \gamma M_z \Delta z \\ L_x = \mu_0 \frac{M_z}{H_z} \frac{\Delta y \Delta z}{\Delta x} \\ L_y = \mu_0 \frac{M_z}{H_z} \frac{\Delta x \Delta z}{\Delta y} \\ R_x = \frac{\mu_0^2 \gamma M_s}{\alpha} \frac{\Delta y \Delta z}{\Delta x} \\ R_y = \frac{\mu_0^2 \gamma M_s}{\alpha} \frac{\Delta x \Delta z}{\Delta y} \end{cases}. \quad (38)$$

It should be noted that (38) differs from (23) in the expressions of the inductances L_x and L_y and the gyrator impedance Z_g . They are no longer constants but functions of M_z and H_z . The values of M_z and H_z depend on the magnitude of excitations and are not explicitly known. A nonlinear inductor over the z-port can be defined likewise:

$$L_z = \mu_0 \frac{M_z}{H_z} \frac{\Delta x \Delta y}{\Delta z}. \quad (39)$$

To construct a nonlinear circuit that is solvable, one may note that

$$\begin{aligned} \frac{M_z}{H_z} &= \frac{M_s}{\sqrt{\left(\frac{H_z}{M_z} M_x \right)^2 + \left(\frac{H_z}{M_z} M_y \right)^2 + H_z^2}} \\ &= \frac{M_s}{\sqrt{\left(\frac{I_{Lx}}{\Delta x} \right)^2 + \left(\frac{I_{Ly}}{\Delta y} \right)^2 + \left(\frac{I^z}{\Delta z} \right)^2}}. \end{aligned} \quad (40)$$

Therefore, the nonlinear gyrator impedance between the x-port and y-port and the nonlinear inductances over all three ports can now be defined as nonlinear functions of the port currents:

$$Z_g = \frac{\mu_0^2 \gamma M_s I^z}{\Delta z \sqrt{\left(\frac{I_{Lx}}{\Delta x} \right)^2 + \left(\frac{I_{Ly}}{\Delta y} \right)^2 + \left(\frac{I^z}{\Delta z} \right)^2}}, \quad (41)$$

$$L_x = \frac{\mu_0 M_s \Delta y \Delta z}{\Delta x \sqrt{\left(\frac{I_{Lx}}{\Delta x} \right)^2 + \left(\frac{I_{Ly}}{\Delta y} \right)^2 + \left(\frac{I^z}{\Delta z} \right)^2}}, \quad (42)$$

$$L_y = \frac{\mu_0 M_s \Delta x \Delta z}{\Delta y \sqrt{\left(\frac{I_{Lx}}{\Delta x} \right)^2 + \left(\frac{I_{Ly}}{\Delta y} \right)^2 + \left(\frac{I^z}{\Delta z} \right)^2}}, \quad (43)$$

$$L_z = \frac{\mu_0 M_s \Delta x \Delta y}{\Delta z \sqrt{\left(\frac{I_{Lx}}{\Delta x} \right)^2 + \left(\frac{I_{Ly}}{\Delta y} \right)^2 + \left(\frac{I^z}{\Delta z} \right)^2}}. \quad (44)$$

The resulting nonlinear circuit model is sketched in Figure 12, which shows mutually coupled nonlinear inductances over all three ports; the x-port and y-port are terminated with dissipation resistances while they are connected through a gyrator.

To incorporate the shape demagnetization, (33) is modified by substituting the demagnetizing terms in

H with (11), which yields equations for the externally applied field:

$$H_y^{\text{appl}} = \frac{H_z^{\text{appl}}}{M_z} M_y + (N_x - N_z) M_y + \frac{\alpha}{\mu_0 \gamma M_s} \frac{\partial M_y}{\partial t} + \frac{1}{\mu_0 \gamma M_z} \frac{\partial M_x}{\partial t} \quad (45a)$$

$$H_x^{\text{appl}} = \frac{H_z^{\text{appl}}}{M_z} M_x + (N_y - N_z) M_x + \frac{\alpha}{\mu_0 \gamma M_s} \frac{\partial M_x}{\partial t} - \frac{1}{\mu_0 \gamma M_z} \frac{\partial M_y}{\partial t} \quad (45b)$$

where H_x^{appl} , H_y^{appl} , and H_z^{appl} represent the scalar components of the externally applied magnetic field. The circuit equivalence, therefore, changes similarly with the introduction of the additional demagnetization term, which becomes

$$I^y = \frac{\int V^y dt}{L_y} + \frac{\int V^y dt}{L_{dy}} + \frac{V^y}{R_y} + \frac{V^x}{Z_g'} \quad (46a)$$

$$I^x = \frac{\int V^x dt}{L_x} + \frac{\int V^x dt}{L_{dx}} + \frac{V^x}{R_x} - \frac{V^y}{Z_g'} \quad (46b)$$

where L_{dx} and L_{dy} are demagnetization inductors that are in shunt with the x -port and y -port inductors, respectively, with their values given by

$$L_{dx} = \frac{\mu_0}{N_x - N_z} \frac{\Delta y \Delta z}{\Delta x} \quad (47a)$$

$$L_{dy} = \frac{\mu_0}{N_y - N_z} \frac{\Delta x \Delta z}{\Delta y} \quad (47b)$$

To set the dc magnetic biasing field, a dc current source is connected to the z -port with the relation of

$$I_{\text{bias}} = H_{\text{bias}} \Delta z, \quad (48)$$

where H_{bias} is the externally applied dc biasing field to the magnetic material.

With these additional inductors, the circuit model is now ready to be used to predict the large-signal behaviors of spin precession in magnetic materials with different shapes, such as thin films, cylinders, and spheres. This is similar to how a nonlinear LLG equation is solved but with reduced complexity and more stability offered by well-developed commercial solvers, such as Keysight ADS.

Two examples are used to validate the proposed circuit model. The first example assumes a YIG sphere that is magnetized in the z -direction. The internal biasing field is set to 80 Oe (6,366 A/m). An external RF field of 0.8 Oe (63.7 A/m) at an FMR frequency of 224 MHz is added in the x -axis to excite the YIG sphere, which increases the transverse magnetization and causes a reduction of the longitudinal magnetization. The simulation results are displayed

This is similar to how a nonlinear LLG equation is solved but with reduced complexity and more stability offered by well-developed commercial circuit solvers, such as Keysight ADS.

in Figure 13, which shows that the x - and y -magnetization components rise at the Larmor precession frequency of 224 MHz with a reduction of the longitudinal magnetization versus time. The comparison concluded that the ADS circuit model provides an accurate prediction of the large-signal behavior of spin precession that is almost identical to that of the LLG equation solver.

The second case is a YIG thin film that is biased in one of its in-plane directions with the y -axis pointing out of the film plane. The biasing field is applied, and the RF excitation is introduced in the same way as in the first example. Because of the out-of-plane demagnetization, the precession is dominantly limited to in plane with its x -component of magnetization much greater than its y -component, which oscillates at the precession frequency given by (14), which is 1.07 GHz. In addition to the reduction of the magnitude, the oscillation of the longitudinal magnetization at twice the FMR frequency is observed. The three-port circuit model shown in Figure 12 is modified with an additional shunt inductor at the y -port to represent the demagnetization. Simulation results with both the MATLAB LLG solver and ADS circuit model display the expected trend, as shown in Figure 14, and the agreement is again very good. It should also be noted in Figure 13 that the z -component of magnetization, in

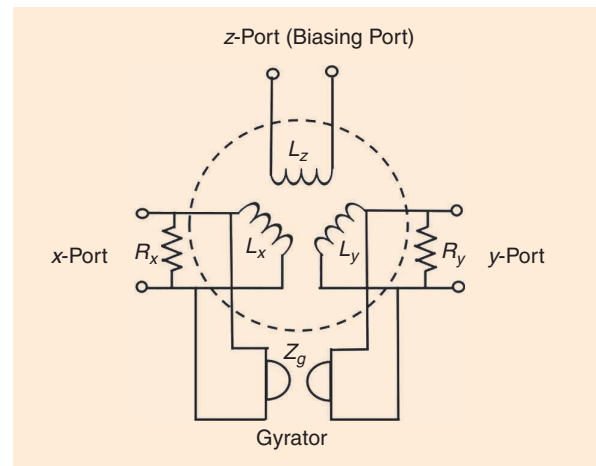


Figure 12. A three-port nonlinear circuit model representing the dynamic spin precession behaviors.

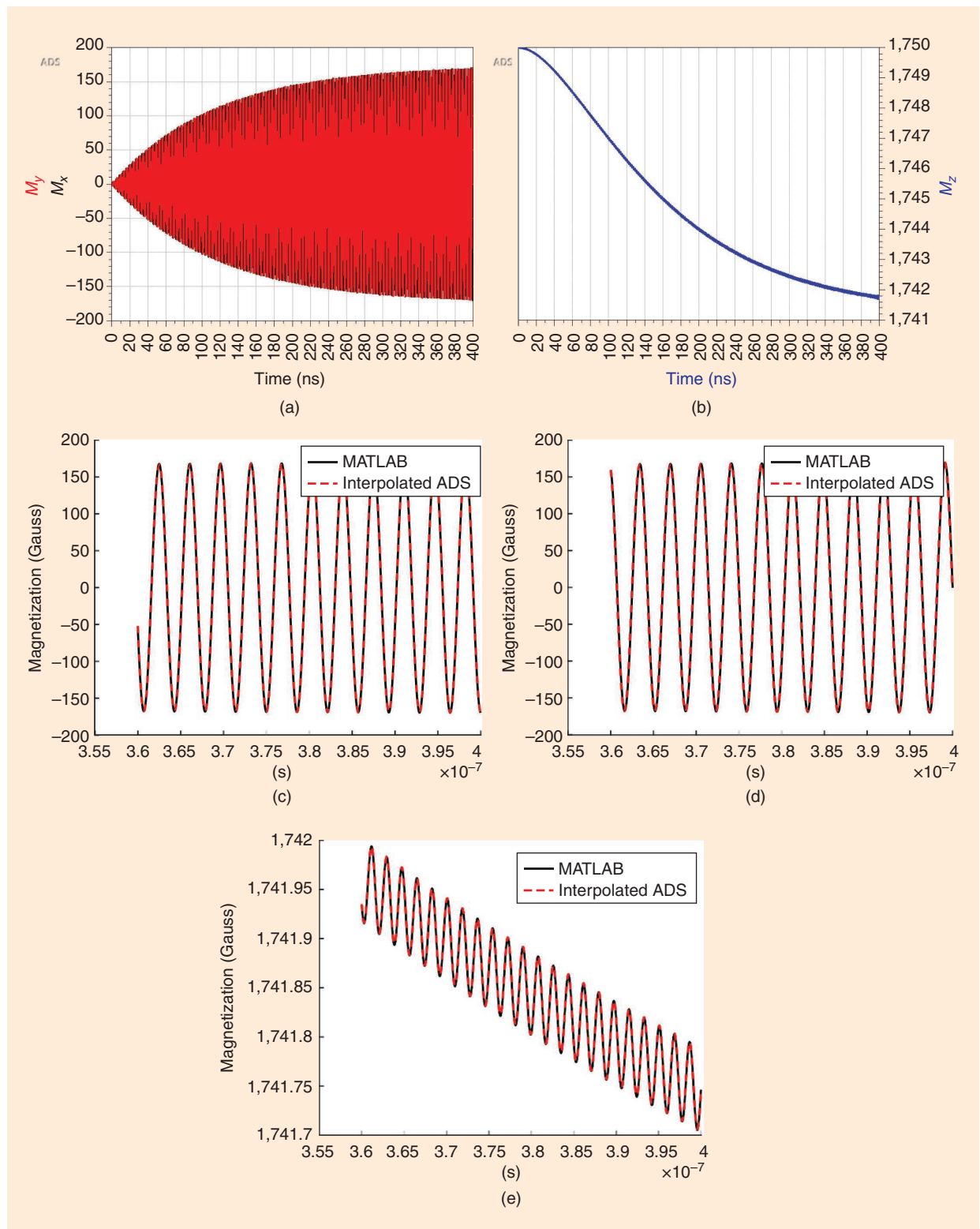


Figure 13. An ADS simulation with the proposed circuit model for a YIG sphere in comparison with an LLG equation solver coded in MATLAB. The spherical geometry has demagnetization coefficients ($N_x = N_y = N_z = 1/3$). (a) MATLAB simulated trajectory of x (black) and y (red) magnetization components versus time. (b) MATLAB simulated trajectory of z-magnetization component versus time. (c), (d), (e) MATLAB (black) and ADS (red) trajectories for x-, y-, and z-magnetization components, respectively; $\alpha = 5e-3$, excitation = $(H_0)1e-3$.

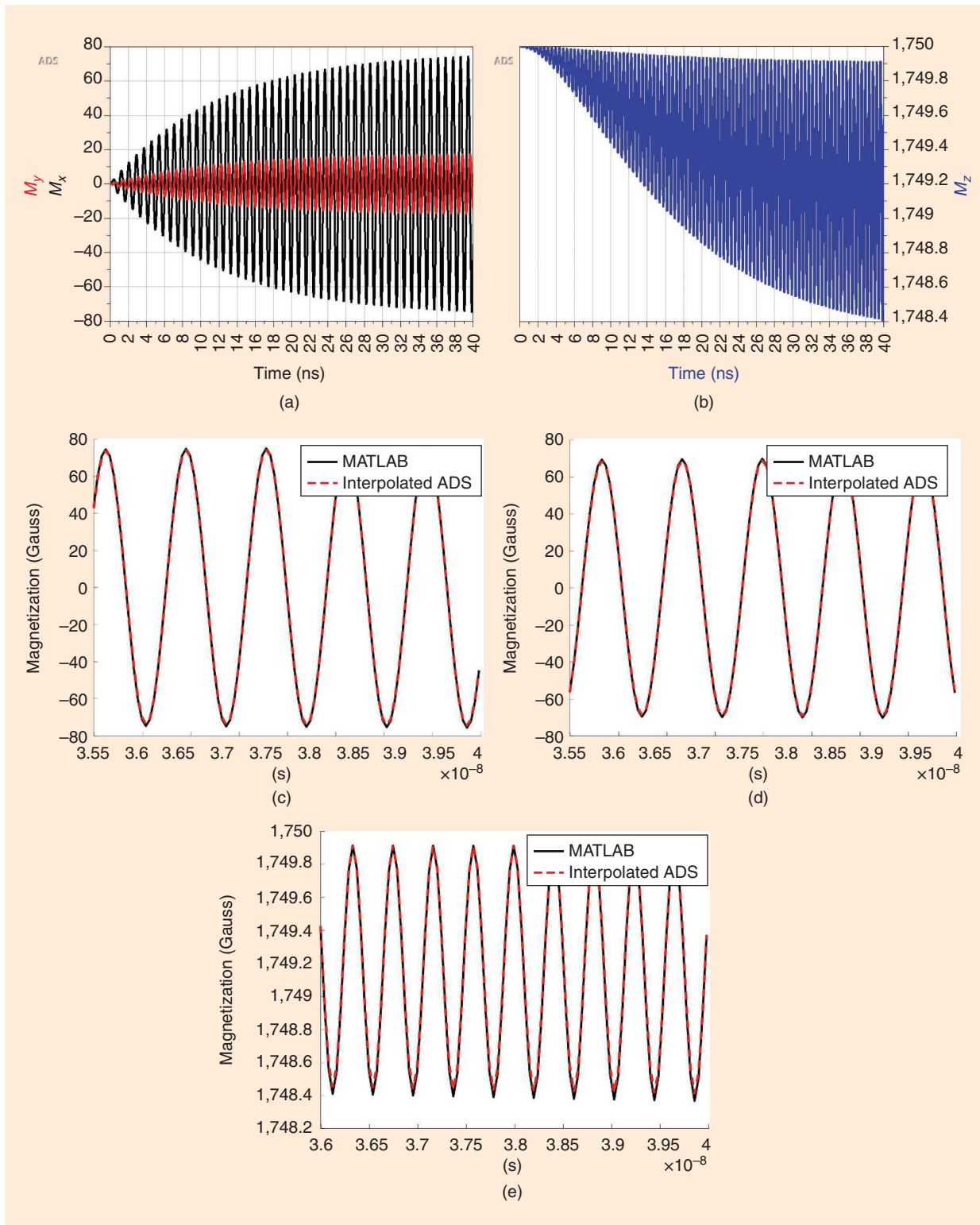


Figure 14. An ADS simulation with the proposed circuit model for a YIG thin film in comparison with an LLG equation solver coded in MATLAB. The thin film has demagnetization coefficients ($N_x = N_z = 0$, $N_y = 1$). (a) MATLAB simulated trajectory of x (black) and y (red) magnetization components versus time. (b) MATLAB simulated trajectory of z-magnetization component versus time. (c), (d), (e). MATLAB (black) and ADS (red) trajectories for x-, y-, and z-magnetization components, respectively; $\alpha = 5e-3$, excitation = $(H_0)1e-3$.

addition to decaying, displays an oscillation behavior at the second harmonic of the precession frequency. This is again predicted by both the LLG solver and the ADS circuit model.

A similar, but simpler, two-port version of the equivalent circuit model for thin films was derived in [14], which describes the in-plane spin precession through an analogy to the motion of a pendulum. The three-port model presented here is more complete and can be universally applied to materials with different shapes.

Equivalent Circuit Models for Magnetostatic Waves and Spin Waves

Magnetostatic waves are approximations of electromagnetic waves within the magnetostatic limit, which applies when the scale of consideration is much shorter than the wavelength of electromagnetic waves in a nondispersive medium. Under such an approximation, the displacement currents in Maxwell's equations are ignored. When only magnetic fields of Maxwellian origin are considered, the lossless form of the LLG equation (8) can be rewritten as

$$\begin{bmatrix} h_x^{\text{appl}} \\ h_y^{\text{appl}} \end{bmatrix} = \frac{1}{\omega_m} \begin{bmatrix} \omega_0 & j\omega \\ -j\omega & \omega_0 \end{bmatrix} \begin{bmatrix} m_x \\ m_y \end{bmatrix} - \begin{bmatrix} h_x^{\text{demag}} \\ h_y^{\text{demag}} \end{bmatrix}. \quad (49)$$

Considering a plane wave propagating in the yz -plane in an infinite biased ferrite, the demagnetization field representing the dipolar coupling is the solution of the sourceless Maxwell equations, which are approximated to be $\nabla \times H = 0$, $\nabla \cdot B = 0$. The solution is

$$\begin{bmatrix} h_x^{\text{demag}} \\ h_y^{\text{demag}} \end{bmatrix} = \begin{bmatrix} 0 & 0 \\ 0 & -\sin^2\theta \end{bmatrix} \begin{bmatrix} m_x \\ m_y \end{bmatrix}, \quad (50)$$

where θ is the angle between the directions of the wave propagation and the dc bias field. The magnetostatic waves are then described by

$$\begin{bmatrix} h_x^{\text{appl}} \\ h_y^{\text{appl}} \end{bmatrix} = \frac{1}{\omega_m} \begin{bmatrix} \omega_0 & j\omega \\ -j\omega & \omega_0 + \omega_m \sin^2\theta \end{bmatrix} \begin{bmatrix} m_x \\ m_y \end{bmatrix}. \quad (51)$$

Setting the applied magnetic field to zero, a non-trivial solution of magnetization exists only when the determinant of the matrix in (51) is zero. This yields the dispersion relation, which is called *Walker's equation*,

$$\omega = [\omega_0(\omega_0 + \omega_m \sin^2\theta)]^{\frac{1}{2}}, \quad (52)$$

where the wavelength dependency disappears.

If the plane wave's H-field is polarized in the x -direction, and it is traveling toward the y -axis, applying $\theta = \pi/2$ and assuming $h_y^{\text{appl}} = 0$ in (51) leads to

$$h_x^{\text{appl}} = \frac{\omega_0(\omega_m + \omega_0) - \omega^2}{\omega_m(\omega_m + \omega_0)} m_x. \quad (53)$$

The previously derived equivalent circuit in Figure 4(b) can thus be used to represent such a plane wave, as shown in Figure 15(a). The magnetostatic approximation is used to neglect the displacement currents, i.e., the shunt capacitances in the circuit model, which results in the equivalent circuit in Figure 15(b). It is evident that the resonant frequency of the structure in Figure 15(b) does not depend on the phase distribution among the different unit cells, which implies a

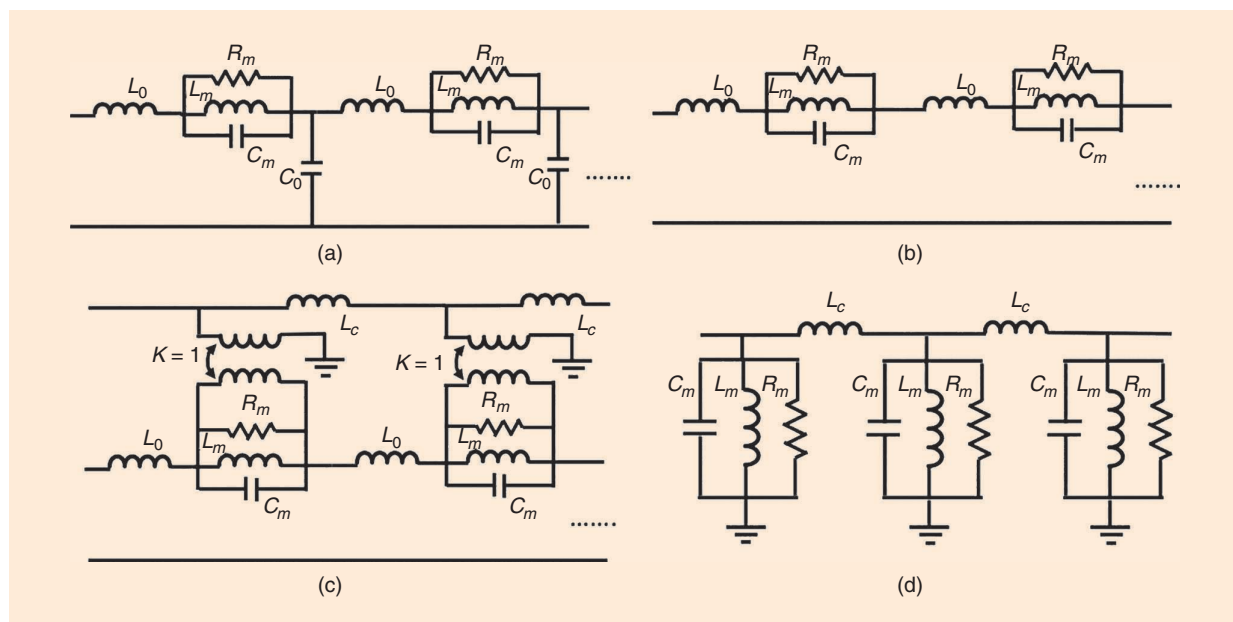


Figure 15. Equivalent circuits for waves traveling in an unbound, biased ferrite. (a) A plane wave traveling perpendicular to the biasing direction, (b) with a magnetostatic wave approximation applied, (c) with exchange coupling included, and (d) with exchange coupling included and the RLC tank transformed to shunt to ground.

k -independent dispersion, as shown by (52). This independence, however, no longer holds when spin waves with exchange coupling are considered [19].

Spin waves are oscillations of magnetizations in the form of waves caused by exchange coupling that has a quantum mechanics origin [42], [43]. The exchange interactions are superimposed with electromagnetic interactions to support the propagation of spin waves at wavelengths much shorter than the electromagnetic wavelengths. This can be represented by including an additional term of the exchange field in Walker's equation [43], which is

$$\begin{bmatrix} h_x^{\text{appl}} \\ h_y^{\text{appl}} \end{bmatrix} = \frac{1}{\omega_m} \begin{bmatrix} \omega_0 & j\omega \\ -j\omega & \omega_0 + \omega_m \sin^2 \theta \end{bmatrix} \begin{bmatrix} m_x \\ m_y \end{bmatrix} - \begin{bmatrix} h_x^{\text{ex}} \\ h_y^{\text{ex}} \end{bmatrix}. \quad (54)$$

The exchange effective field can be defined either from quantum theory or in a classical form [43]. The quantum theory takes the quantized form

$$\begin{bmatrix} h_x^{\text{ex}} \\ h_y^{\text{ex}} \end{bmatrix} = -\frac{2\lambda_{\text{ex}}}{a^2} \begin{bmatrix} 1 - \cos(ka) & 0 \\ 0 & 1 - \cos(ka) \end{bmatrix} \begin{bmatrix} m_x \\ m_y \end{bmatrix}, \quad (55)$$

where k is the propagation constant of the spin wave, a is the lattice constant ($a = 1.2$ nm for the YIG), and λ_{ex} is the exchange constant ($\lambda_{\text{ex}} = 3 \times 10^{-16}$ m² for the YIG [19]). The classical form of the effective field that is more frequently used is

$$\begin{bmatrix} h_x^{\text{ex}} \\ h_y^{\text{ex}} \end{bmatrix} = \lambda_{\text{ex}} \begin{bmatrix} \nabla^2 & 0 \\ 0 & \nabla^2 \end{bmatrix} \begin{bmatrix} m_x \\ m_y \end{bmatrix}. \quad (56)$$

One can easily prove that these two definitions are equivalent for spin waves with wavelengths much larger than the lattice constant. Combining (53) and (55) suggests that the exchange effect can be added to the dispersion relation by replacing ω_0 by $[\omega_0 + 2\omega_m \lambda_{\text{ex}} (1 - \cos ka) / a^2]$ in (53):

$$\omega = \left(\omega_0 + \omega_m \frac{2\lambda_{\text{ex}}}{a^2} (1 - \cos(ka)) \right)^{\frac{1}{2}} \times \left(\omega_0 + \omega_m \frac{2\lambda_{\text{ex}}}{a^2} (1 - \cos(ka)) + \omega_m \sin^2 \theta \right)^{\frac{1}{2}}. \quad (57)$$

Expanding the preceding equation with $\theta = \pi/2$ and ignoring the high-order terms, one obtains

$$\cos(ka) = 1 - \frac{\omega^2 - \omega_0(\omega_0 + \omega_m)}{2\omega_0 + \omega_m} \frac{a^2}{2\omega_m \lambda_{\text{ex}}}. \quad (58)$$

From (56), it is evident that the nature of the exchange coupling is to add an effective magnetic field that is proportional to the differential of the adjacent spins. It is reasonable to represent this relation by coupling inductors, as shown in Figure 15(c). The value of the exchange coupling inductor can be determined by forcing the circuit model to exhibit the same dispersion relation as shown in (58). Assuming no external RF magnetic field is applied, the voltages across the different RLC tanks are independent of each other with the

exception of coupling through the transformers. Therefore, the circuit model representing the magnetization portion in Figure 15(c) is transformed to the one in Figure 15(d), where the RLC tanks are shunt to ground. The dispersion relation can now be easily determined with the periodical structure theory, using the ABCD matrix method [48], as

$$\cos(kd) = 1 - \frac{1}{2\omega^2 L_c C_m} + \frac{L_c}{2L_m}, \quad (59)$$

where d is the distance between each unit, which should be set to the same value as the lattice constant a to replicate the dispersion relation in (58). Under this condition, the expression for the coupling inductance L_c is given by

$$L_c = \frac{d^2}{\lambda_{\text{ex}} \omega_m} \frac{\omega_0(\omega_0 + \omega_m)}{2\omega_0 + \omega_m} L_m. \quad (60)$$

The equivalent circuit depicted in Figure 15(d) is now complete and can be used to predict the dispersive behavior of the spin wave. Similar periodic circuit models have been used to represent other types of linear or nonlinear waves [50], [51].

The dispersion relation formulated in (58) is plotted in Figure 16, and it is evident that k -independence no longer holds for high- k or short-wavelength waves, where it corresponds to a frequency much higher than the FMR.

One practical concern is that since the lattice constant a is at nanometers, modeling the entire dispersion curve with a periodic circuit model described by (59) and (60) would require $d = a$, and an overwhelmingly large number of unit cells would have to be used to represent a millimeter-long magnetic material structure. However, if one aims at replicating only the bottom portion of the dispersion curve, a much coarser

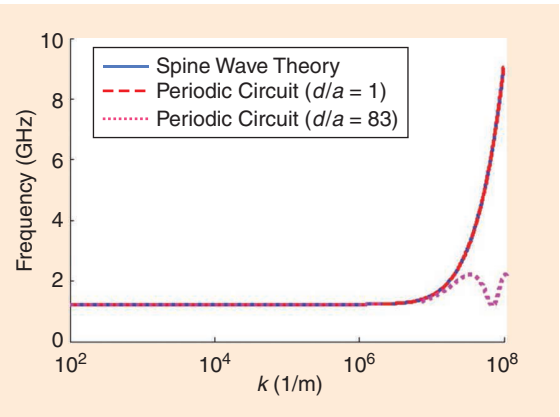


Figure 16. A comparison of the dispersion curve calculated from spin wave theory by (51) to the ones calculated from the periodic circuit in Figure 14 with 1.2 nm ($d/a = 1$) and 100 nm thicknesses ($d/a = 83$) for each unit using (53). (Source: [14].)

spatial discretization may be used as the distance resolution d determines the maximum spin-wave frequency the circuit model can cover. Figure 16 compares the analytical spin-wave dispersion relation derived from (58) to the curve derived from the periodic circuit with (59) on different ratios of spatial resolution d versus lattice constant a . When the spatial resolution in each resonator ($R_m L_m C_m$ parallel circuit) is close to the lattice constant (e.g., 1.2 nm), the circuit model is able to include very high-frequency spin waves. When the thickness resolution is made much coarser than the lattice constant (e.g., 100 nm), the circuit model shows a cutoff frequency without capturing the higher frequency spin waves. Yet the lower frequency end of the dispersion is still well represented. This implies that the computational complexity can be much reduced by using coarser spatial discretization if only the long-wavelength spin waves or those with frequencies close to the FMR are of interest.

Nonlinear Equivalent Circuit Model for FSLs

The spin-wave model presented in Figure 14(d) can be combined with the nonlinear dynamic precession model in Figure 12 to form a complete equivalent circuit model for nonlinear RF magnetic devices, such as FSLs, to predict their large-signal behaviors, such as power-dependent insertion loss, frequency selectivity, intermodulations, and transient responses, in a way similar to what was done in [44].

An FSL device is often made by sandwiching the center strip of a stripline with two layers of YIG film or substrate with a bias field parallel to the RF magnetic field [30]. When a small signal of interest goes through the FSL along with a large-signal interferer, the FSL attenuates only the large signals that are above its threshold while letting the weak useful signal pass without attenuation. The bottom half of the stripline

structure is illustrated in Figure 17, which shows an RF wave traveling toward the longitudinal direction exciting spin-wave oscillations along the thickness of the YIG substrate. Figure 17 also shows a possible discretization strategy for modeling, which divides the transmission line into multiple segments in its longitudinal direction. For each segment, the current passing through the stripline feeds the RF energy to the oscillation of the spin waves along the thickness direction through the nonlinear spin precession model presented in the section “Nonlinear Equivalent Circuit Model for Dynamic Spin Precession,” while the propagation of the spin waves between the two thickness boundaries can be represented by the spin-wave equivalent circuit in Figure 15(d).

The resulting equivalent circuit for the entire FSL device is thus yielded as depicted in Figure 18, which consists of an LC ladder network that represents the transmission line but with the insertion of the nonlinear spin unit into each LC unit. In each nonlinear spin unit, multiple three-port spin precession models are used, while each of them represents a subdivision along the thickness direction. The y -ports of all of the spin precession models are terminated with a demagnetization inductor to represent the out-of-plane shape demagnetization. The x -ports of the spin precession models are interconnected through a coupling inductor, which represents the exchange coupling, while all of the z -ports of the spin precession model are fed by the same dc current source, which represents the dc biasing field. The z -ports are also excited by a common RF current, which represents the RF magnetic field under the center strip, which is approximately uniform over the cross section of the stripline.

Such a model is used to predict the performance of the FSL device presented in [30]. The stripline is 25 μm

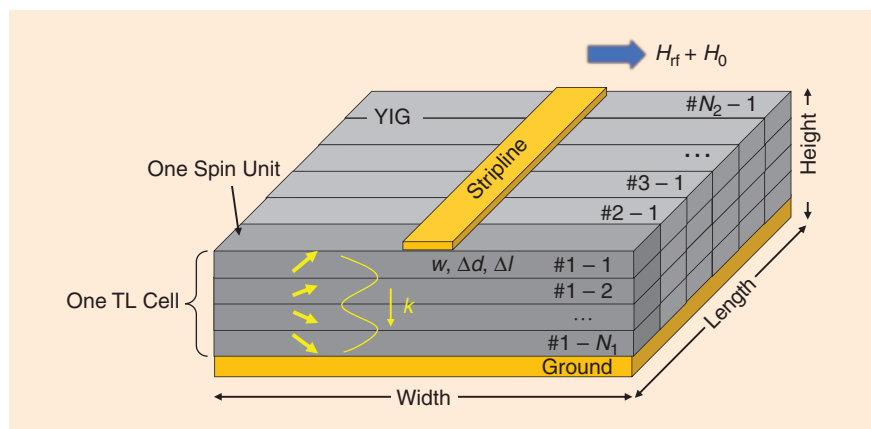


Figure 17. A stripline FSL device structure that shows spin-wave oscillations launched along the thickness direction under the excitation of the RF wave traveling in the transmission line. TL: transmission line. (Source: [44].)

wide, and the conductor is sandwiched by two layers of 100- μm -thick, 200- μm -wide single-crystal YIG. The total length of the stripline FSL is 38 mm, and the bias field applied is 100 Oe (7.96×10^3 A/m) in parallel with the RF field. In the circuit model, five divisions in the longitudinal direction and 500 divisions in the thickness directions are used. The circuit parameters are chosen based on (38)–(41) and (57). The dimension parameters are defined as follows. Δz is the width of the ferrite, which is 200 μm , and Δy or d

is the thickness of each division in the thickness direction with an additional factor of $\frac{1}{2}$ to include the upper half of the stripline area, which is $100 \mu\text{m}/500/2 = 100 \text{ nm}$. Δx is the division in the longitudinal direction, which equals $38 \text{ mm}/5 = 7.6 \text{ mm}$. The YIG is assumed to have a saturation magnetization of $1,750 \text{ Oe}$ ($1.39 \times 10^5 \text{ A/m}$) and a Gilbert damping constant of 5×10^{-4} . The entire circuit can be implemented in ADS and simulated with either transient or envelope simulations. The damping resistors in the circuits are assumed to be thermal resistors, and their thermal noise excites the oscillation of spin waves, powered by the RF field through the nonlinear spin precessions. The following four metrics are used to characterize the performance of the FSL device:

- 1) *Limiting threshold*: FSL devices start to attenuate the incoming RF signal when the power is above a certain threshold. This threshold is determined by the linewidth of the YIG material and the strength of the magnetic field, which is often controlled by the width of the center strip.
- 2) *Power-dependent insertion loss*: The attenuation level to the strong signal in the FSL is nonlinear

The circuit models are concise representations of the material physics, and they offer direct insights into the nonreciprocal, dispersive, and nonlinear behaviors of the material.

and depends on its power. A signal with higher power receives greater attenuation.

- 3) *Delay time*: The FSL device requires a certain amount of energy to be established in the spin waves before it starts to attenuate the incoming RF signal, which leads to a delay time of the power-limiting action. This delay time depends on the input power level.
- 4) *Frequency selectivity*: The power-limiting mechanism of the FSL device is coupling of the RF energy of the strong signal to the half-frequency spin-wave oscillations in the material, which behaves as a significant energy loss to the strong signal.

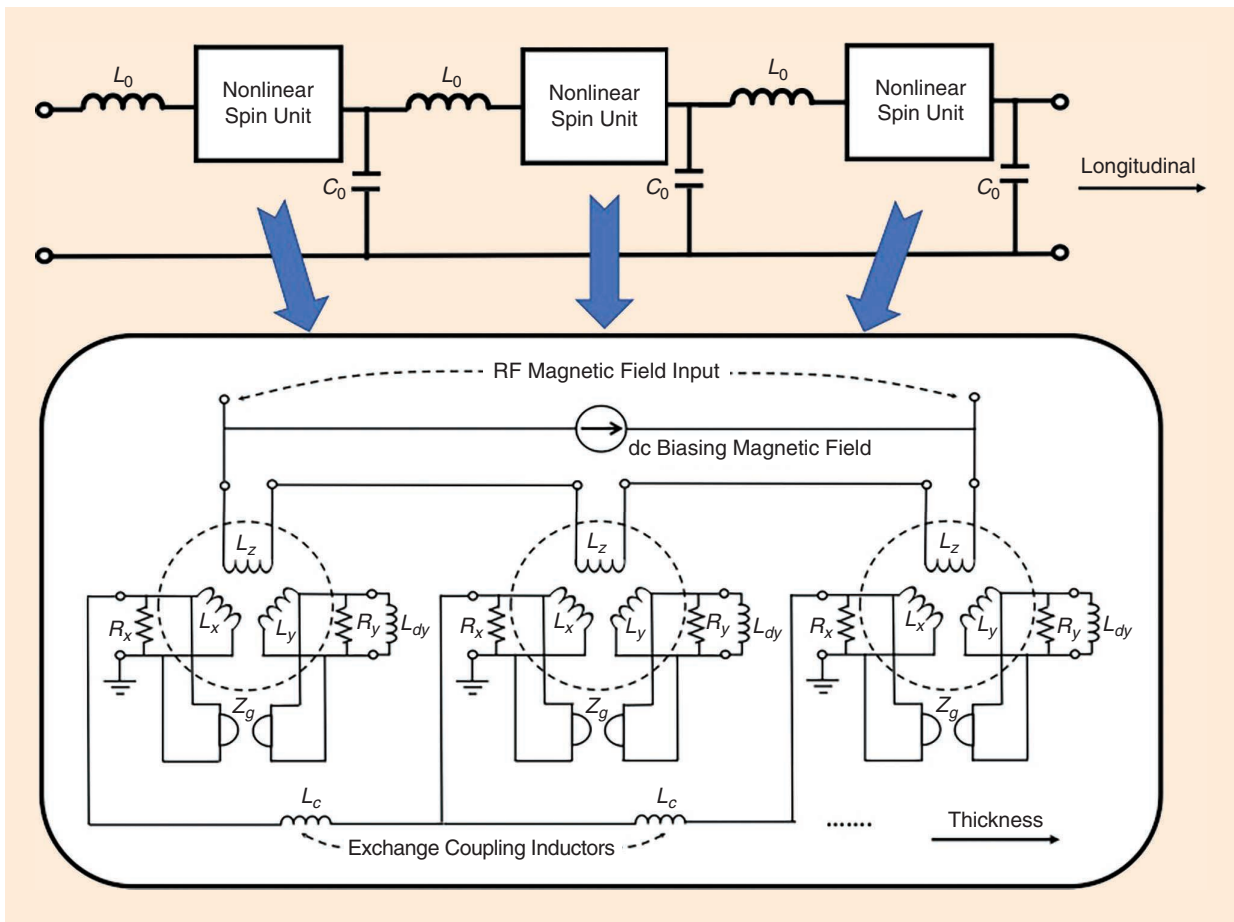


Figure 18. A proposed circuit model in the form of multiple segments of the LC transmission line, where a nonlinear spin unit is inserted into each LC unit. Each nonlinear spin unit consists of a large group of nonlinear spin precession models that are coupled to each other through a series inductor that represents exchange coupling.

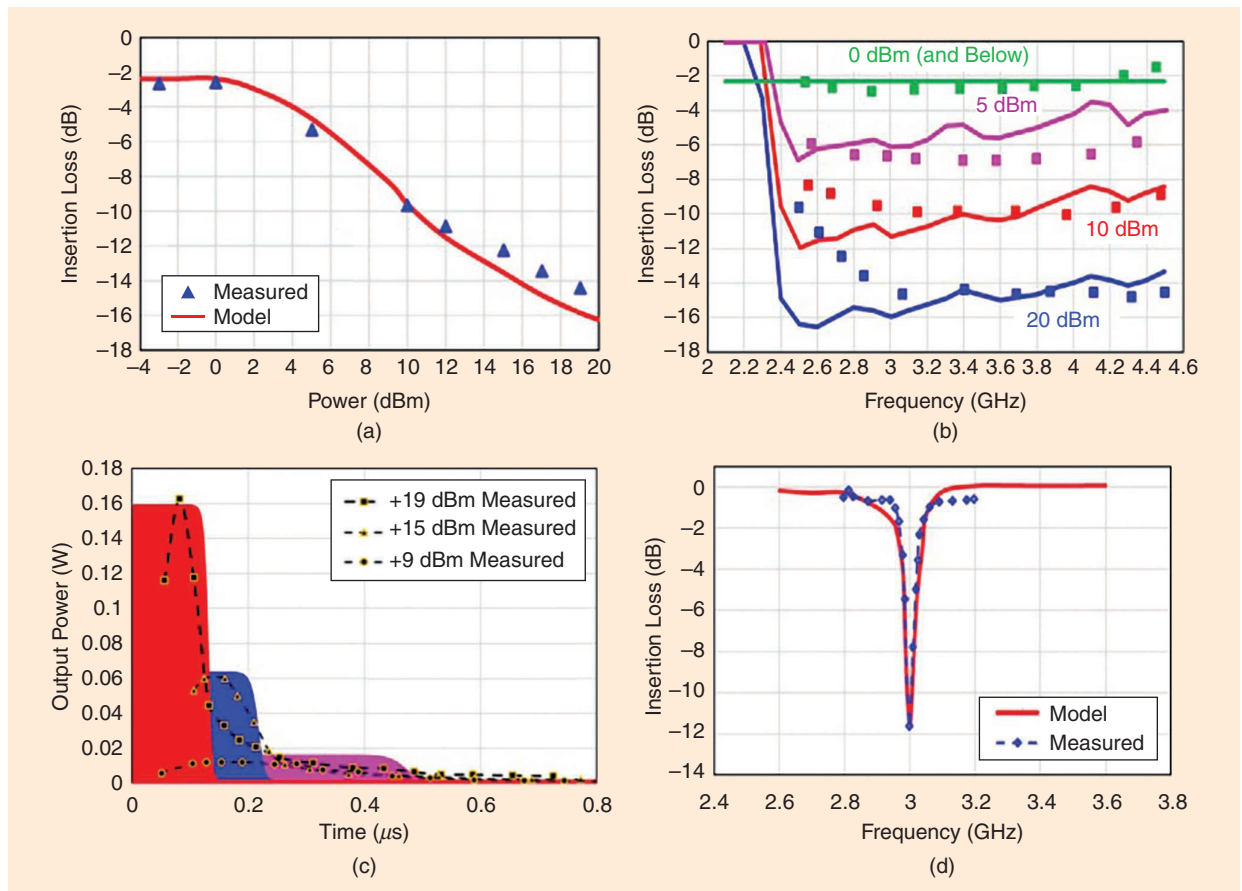


Figure 19. Simulated results for the stripline FSL device with the proposed circuit model, compared to the measured results on the four metrics. (a) Insertion loss versus input power at 3 GHz. (b) Insertion loss versus frequency at four different power levels. (c) Delay time before the power-limiting effect appears. (d) Frequency selectivity when a strong signal presents at 3 GHz.

A weak signal that coexists with the strong signal but at a different frequency should not correlate with the spin-wave oscillations. It will thus not be attenuated in an ideal material with no damping. However, because of the damping of the spin precessions in real material, a certain correlation may be formed when the weak signal frequency is close to the strong signal frequency, which causes absorption to the weak signal. Frequency selectivity characterizes how narrow an absorption band the strong signal creates to the weak signal. The predicted results with the circuit model for the previous four performance metrics are plotted in Figure 19(a)–(d) and compared with the experimental results presented in [30]. Very good agreement is observed for all four metrics, which confirms the effectiveness of the proposed model.

Conclusions

Equivalent circuit models are derived from micromagnetic theory to represent the linear and nonlinear spin precessions and spin-wave propagations in RF magnetic material. The circuit models are concise representations of the material physics, and they offer direct insights into the nonreciprocal, dispersive, and nonlinear behaviors of

the material. The equivalent circuit models for the material can be combined with the circuit models representing other parts of the device to form complete device circuit models that can be used to predict the performance of RF magnetic devices. Examples like ferrite-loaded stripline, ferrite-loaded electrically small antennas, and FSLs have been used to demonstrate the efficacy of these models. Circuit simulations based on these models yielded results that are in good agreement with either full-wave simulations or measured results.

References

- [1] B. Lax and K. J. Button, *Microwave Ferrites and Ferrimagnetics*. New York, NY, USA: McGraw-Hill, 1962.
- [2] U. Ozgur, Y. Alivov, and H. Morkoc, "Microwave ferrites, part 1: Fundamental properties," *J. Mater. Sci. Mater. Electron.*, vol. 20, no. 9, pp. 789–834, 2009, doi: 10.1007/s10854-009-9923-2.
- [3] U. Ozgur, Y. Alivov, and H. Morkoc, "Microwave ferrites, part 2: Passive components and electrical tuning," *J. Mater. Sci. Mater. Electron.*, vol. 20, no. 10, pp. 911–952, 2009, doi: 10.1007/s10854-009-9924-1.
- [4] R. Soohoo, "Microwave ferrite materials and devices," *IEEE Trans. Magn.*, vol. 4, no. 2, pp. 118–133, Jun. 1968, doi: 10.1109/TMAG.1968.1066207.
- [5] J. D. Adam, L. E. Davis, G. F. Dionne, E. F. Schloemann, and S. N. Stitzer, "Ferrite devices and materials," *IEEE Trans. Microw. Theory Techn.*, vol. 50, no. 3, pp. 721–737, Mar. 2002, doi: 10.1109/22.989957.

- [6] T. Kuribara, M. Yamaguchi, and K. Arai, "Equivalent circuit analysis of an RF integrated ferromagnetic inductor," *IEEE Trans. Magn.*, vol. 38, no. 5, pp. 3159–3161, Sep. 2002, doi: 10.1109/TMAG.2002.802400.
- [7] E. N. Skomal, "Theory of operation of a 3-port Y-junction ferrite circulator," *IEEE Trans. Microw. Theory Techn.*, vol. 11, no. 2, pp. 117–122, Mar. 1963, doi: 10.1109/TMTT.1963.1125612.
- [8] C. E. Fay and R. L. Comstock, "Operation of the ferrite junction circulator," *IEEE Trans. Microw. Theory Techn.*, vol. 13, no. 1, pp. 15–27, Jan. 1965, doi: 10.1109/TMTT.1965.1125923.
- [9] E. K.-N. Yung, R. S. Chen, K. Wu, and D. X. Wang, "Analysis and development of millimeter-wave waveguide-junction circulator with a ferrite sphere," *IEEE Trans. Microw. Theory Techn.*, vol. 46, no. 11, pp. 1721–1734, Nov. 1998, doi: 10.1109/22.734570.
- [10] P. Shi, H. How, X. Zuo, S. D. Yoon, S. A. Oliver, and C. Vittoria, "MMIC circulators using hexaferrites," *IEEE Trans. Magn.*, vol. 37, no. 4, pp. 2389–2391, Jul. 2001, doi: 10.1109/20.951181.
- [11] B. N. Enander, "A new ferrite isolator," *Proc. IRE*, vol. 44, no. 10, pp. 1421–1430, Oct. 1956, doi: 10.1109/JRPROC.1956.274986.
- [12] P. S. Carter, "Magnetically-tunable microwave filters using single-crystal yttrium-iron-garnet resonators," *IRE Trans. Microw. Theory Techn.*, vol. 9, no. 3, pp. 252–260, May 1961, doi: 10.1109/TMTT.1961.1125316.
- [13] J. Uher and W. J. R. Hoefer, "Tunable microwave and millimeter-wave band-pass filters," *IEEE Trans. Microw. Theory Techn.*, vol. 39, no. 4, pp. 643–653, Apr. 1991, doi: 10.1109/22.76427.
- [14] J. Helszajn, *YIG Resonators and Filters*. New York, NY, USA: Wiley, 1985.
- [15] H. Tanbakuchi, D. Nicholson, B. Kunz, and W. Ishak, "Magnetically tunable oscillators and filters," *IEEE Trans. Magn.*, vol. 25, no. 5, pp. 3248–3253, Sep. 1989, doi: 10.1109/20.42268.
- [16] Y.-Y. Song, Y. Sun, L. Lu, J. Bevivino, and M. Wu, "Self-biased planar millimeter wave notch filters based on magnetostatic wave excitation in barium hexagonal ferrite thin films," *Appl. Phys. Lett.*, vol. 97, no. 17, p. 173,502, 2010, doi: 10.1063/1.3504256.
- [17] L. Lu, Y.-Y. Song, J. Bevivino, and M. Wu, "Planar millimeter wave band-stop filters based on the excitation of confined magnetostatic waves in barium hexagonal ferrite thin film strips," *Appl. Phys. Lett.*, vol. 98, no. 21, p. 212,505, 2011, doi: 10.1063/1.3592817.
- [18] S. Dai, S. A. Bhavne, and R. Wang, "Octave-tunable magnetostatic wave YIG resonators on a chip," *IEEE Trans. Ultrason., Ferroelectr., Freq. Control*, vol. 67, no. 11, pp. 2454–2460, 2020, doi: 10.1109/TUFFC.2020.3000055.
- [19] A. D. Brown, J. L. Volakis, L. C. Kempel, and Y. Botros, "Patch antennas on ferromagnetic substrates," *IEEE Trans. Antennas Propag.*, vol. 47, no. 1, pp. 26–32, Jan. 1999, doi: 10.1109/8.752980.
- [20] G. Yang *et al.*, "Tunable miniaturized patch antennas with self-biased multilayer magnetic films," *IEEE Trans. Antennas Propag.*, vol. 57, no. 7, pp. 2190–2193, Jul. 2009, doi: 10.1109/TAP.2009.2021972.
- [21] M. Sigalov, R. Shavit, R. Joffe, and E. O. Kamenetskii, "Manipulation of the radiation characteristics of a patch antenna by small ferrite disks inserted in its cavity domain," *IEEE Trans. Antennas Propag.*, vol. 61, no. 5, pp. 2371–2379, May 2013, doi: 10.1109/TAP.2013.2242830.
- [22] V. G. Kononov, C. A. Balanis, and C. R. Birtcher, "The impact of non-uniform bias field on the radiation patterns of ferrite-loaded CBS antennas," *IEEE Trans. Antennas Propag.*, vol. 61, no. 8, pp. 4367–4371, Aug. 2013, doi: 10.1109/TAP.2013.2259452.
- [23] W. Gu, K. Luong, Z. Yao, H. Cui, and Y. E. Wang, "Ferromagnetic resonance enhanced electrically small antennas," *IEEE Trans. Antennas Propag.*, vol. 69, no. 12, pp. 8304–8314, Dec. 2021, doi: 10.1109/TAP.2021.3090032.
- [24] K. L. Kotzebue, "Frequency-selective limiting in YIG filters," *J. Appl. Phys.*, vol. 33, no. 2, p. 747, 1962, doi: 10.1063/1.1702502.
- [25] S. S. Elliott, "A broadband ferrite limiter," in *Proc. AIP Conf.*, 1974, vol. 18, p. 1273, doi: 10.1063/1.2947257.
- [26] J. Brown, "Ferromagnetic limiters," *Microw. J.*, vol. 4, pp. 74–79, Nov. 1961.
- [27] P. R. Emtage and S. N. Stitzer, "Interaction of signals in ferromagnetic microwave limiters," *IEEE Trans. Microw. Theory Techn.*, vol. 25, no. 3, pp. 210–213, Mar. 1977, doi: 10.1109/TMTT.1977.1129072.
- [28] J. Adam, "A broadband microwave signal to noise enhancer," *IEEE Trans. Magn.*, vol. 16, no. 5, pp. 1168–1170, Sep. 1980, doi: 10.1109/TMAG.1980.1060801.
- [29] S. Stitzer, "Frequency selective microwave power limiting in thin YIG films," *IEEE Trans. Magn.*, vol. 19, no. 5, pp. 1874–1876, Sep. 1983, doi: 10.1109/TMAG.1983.1062773.
- [30] J. D. Adam and S. N. Stitzer, "Frequency selective limiters for high dynamic range microwave receivers," *IEEE Trans. Microw. Theory Techn.*, vol. 41, no. 12, pp. 2227–2231, Dec. 1993, doi: 10.1109/22.260710.
- [31] T. Nomoto and Y. Matsushita, "A signal-to-noise enhancer using two MSSW filters and its application to noise reduction in DBS reception," *IEEE Trans. Microw. Theory Techn.*, vol. 41, no. 8, pp. 1316–1322, Aug. 1993, doi: 10.1109/22.241669.
- [32] S. M. Gillette, M. Geiler, J. D. Adam, and A. L. Geiler, "Ferrite-based reflective-type frequency selective limiters," in *Proc. IEEE MTT-S Int. Microw. Workshop Ser. Adv. Mater. Process. RF THz Appl. (IMWS-AMP)*, Ann Arbor, MI, USA, 2018, pp. 1–3, doi: 10.1109/IMWS-AMP.2018.8457134.
- [33] Y. Cui *et al.*, "Monolithic integration of self-biased C-Band circulator on SiC substrate for GaN MMIC applications," *IEEE Electron Device Lett.*, vol. 40, no. 8, pp. 1249–1252, Aug. 2019, doi: 10.1109/LED.2019.2921090.
- [34] "Ansys electronics desktop," Ansys Corporation, Pittsburgh, PA, USA, Suite v18, 2017.
- [35] "The object oriented micromagnetic framework project at IITL/NIST," NIST, Gaithersburg, MD, USA, 2021. [Online]. Available: <https://math.nist.gov/oommf/>
- [36] M. J. Donahue and D. G. Porter, *OOMMF User's guide*. U.S. Department of Commerce, Technology Administration, National Institute of Standards and Technology, Washington, DC, USA, 1999.
- [37] R. Chang, S. Li, M. V. Lubarda, B. Livshitz, and V. Lomakina, "FastMag: Fast micromagnetic simulator for complex magnetic structures," *J. Appl. Phys.*, vol. 109, no. 7, p. 07D358, 2011, doi: 10.1063/1.3563081.
- [38] S. Fu, W. Cui, M. Hu, R. Chang, M. J. Donahue, and V. Lomakin, "Finite-Difference micromagnetic solvers with the Object-Oriented Micromagnetic Framework on graphics processing units," *IEEE Trans. Magn.*, vol. 52, no. 4, pp. 1–9, Apr. 2016, Art. no. 7100109, doi: 10.1109/TMAG.2015.2503262.
- [39] A. Vansteenkiste and B. Van de Wiele, "MuMax: A new high-performance micromagnetic simulation tool," *J. Magn. Magn. Mater.*, vol. 323, no. 21, pp. 2585–2591, 2011, doi: 10.1016/j.jmmm.2011.05.037.
- [40] D. Wei, *Micromagnetics and Recording Materials*. Berlin, Germany: Springer-Verlag, 2012.
- [41] A. A. Serga, A. V. Chumak, and B. Hillebrands, "YIG magnonics," *J. Phys. D, Appl. Phys.*, vol. 43, no. 26, p. 264,002, 2010, doi: 10.1088/0022-3727/43/26/264002.
- [42] C. Herring and C. Kittel, "On the theory of spin waves in ferromagnetic media," *Phys. Rev.*, vol. 81, no. 5, p. 869, Mar. 1951.
- [43] D. D. Stancil and A. Prabhakar, *Spin Waves: Theory and Applications*. New York, NY, USA: Springer-Verlag, 2009.
- [44] H. Cui, Z. Yao, and Y. E. Wang, "Coupling electromagnetic waves to spin waves: A physics-based nonlinear circuit model for frequency-selective limiters," *IEEE Trans. Microw. Theory Techn.*, vol. 67, no. 8, pp. 3221–3229, Aug. 2019, doi: 10.1109/TMTT.2019.2918517.
- [45] T. Qu *et al.*, "Nonlinear magnon scattering mechanism for microwave pumping in magnetic films," *IEEE Access*, vol. 8, pp. 216,960–216,968, Nov. 2020, doi: 10.1109/ACCESS.2020.3040711.
- [46] T. Qu, A. Venugopal, and R. Victora, "Dependence of nonlinear response and magnon scattering on material properties," *J. Appl. Phys.*, vol. 129, no. 16, p. 163,903, 2021, doi: 10.1063/5.0044925.
- [47] A. Venugopal and R. Victora, "Effective phase noise considerations in magnon based parametric excitations," *Sci. Rep.*, vol. 11, May 2021, Art. no. 11322, doi: 10.1038/s41598-021-90730-5.
- [48] D. M. Pozar, *Microwave Engineering*, 3rd ed. Hoboken, NJ, USA: Wiley, 2005.
- [49] L. J. Chu, "Physical limitations of omni-directional antennas," *J. Appl. Phys.*, vol. 35, pp. 1479–1484, May 1964.
- [50] W. H. Louisell, *Coupled Mode and Parametric Electronics*. New York, NY, USA: Wiley, 1960.
- [51] A. Scott, *Active and Nonlinear Wave Propagation in Electronics*. New York, NY, USA: Wiley, 1970.

